

# Nesprin-1 role in DNA damage response

Ilknur Sur, Sascha Neumann, and Angelika A Noegel\*

Institute of Biochemistry I; Medical Faculty; Center for Molecular Medicine Cologne (CMMC) and Cologne Excellence Cluster on Cellular Stress Responses in Aging-Associated Diseases (CECAD); University of Cologne; Cologne, Germany

**Keywords:** nuclear envelope, Nesprin-1, DNA damage repair, MutS $\alpha$ , cancer

Nuclear envelope (NE) proteins have fundamental roles in maintaining nuclear structure, cell signaling, chromatin organization, and gene regulation, and mutations in genes encoding NE components were identified as primary cause of a number of age associated diseases and cancer. Nesprin-1 belongs to a family of multi-isomeric NE proteins that are characterized by spectrin repeats. We analyzed NE components in various tumor cell lines and found that Nesprin-1 levels were strongly reduced associated with alterations in further NE components. By reducing the amounts of Nesprin-1 by RNAi mediated knockdown, we could reproduce those alterations in mouse and human cell lines. In a search for novel Nesprin-1 binding proteins, we identified MSH2 and MSH6, proteins of the DNA damage response pathway, as interactors and found alterations in the corresponding pathways in cells with lower Nesprin-1 levels. We also noticed increased number of  $\gamma$ H2AX foci in the absence of exogenous DNA damage as was seen in tumor cells. The levels of phosphorylated kinases Chk1 and 2 were altered in a manner resembling tumor cells and the levels of Ku70 were low and the protein was not recruited to the DNA after hydroxyurea (HU) treatment. Our findings indicate a role for Nesprin-1 in the DNA damage response pathway and propose Nesprin-1 as novel player in tumorigenesis and genome instability.

## Introduction

The chromosomes in eukaryotic cells are separated from the cytoplasm by a selective barrier, the NE, which regulates nucleo-cytoplasmic traffic and connects the nucleoplasm to the cytoplasm.<sup>1,2</sup> The NE consists of an outer (ONM) and inner nuclear membrane (INM) that enclose the perinuclear space (PNS). The ONM is contiguous with the endoplasmic reticulum; the INM contacts the nuclear lamina and chromatin. Nuclear pore complexes are inserted into the NE and connect the nucleus with the cytoplasm. The protein composition of the NE is complex as more than 100 proteins have been described and differs between the ONM and INM.<sup>3</sup> These proteins are involved in a variety of cellular processes including genome organization, gene expression, and stability.<sup>4,5</sup>

Nesprins are components of a characteristic NE protein assembly, the LINC (linker of nucleoskeleton and cytoskeleton) complex that connects the nucleus with the cytoskeleton. It consists of Nesprins in the ONM and SUN proteins in the INM which interact in the PNS.<sup>6</sup> Disruption of the nuclear-cytoskeletal connection has severe consequences: The stability, size, and shape of the nucleus are altered, its position in the cell is disturbed, cell migration is affected, and the mechanical properties of the cell and mechanotransduction from the extracellular space to the nucleus are impaired as well as signaling processes. The importance is further underlined by the large group of laminopathies in which components of the nuclear lamina and the NE are mutated, generating a variety of degenerative diseases affecting striated

muscle and peripheral nerves, skeletal, and fat development, and premature aging syndromes.<sup>1,2</sup>

Mutations in the *SYNE1* gene encoding Nesprin-1 have been identified in some forms of Emery-Dreifuss muscular dystrophy, cerebellar ataxia, and arthrogryposis.<sup>7–9</sup> Analysis of Nesprin-1 knockout mice showed roles in nuclear morphology, NE organization, actin organization, and cell motility,<sup>10–14</sup> and in vitro studies demonstrated that knockdown of Nesprin-1 led to nuclear defects and mislocalization of Emerin and SUN2 in U2OS and fibroblast cells.<sup>7</sup> Downregulation of Drop1, an N-terminal isoform of Nesprin-1, has been observed in early tumor stages in a wide range of human carcinomas.<sup>15</sup> Furthermore, mutations in *SYNE1* were observed in ovarian and colorectal cancers.<sup>16,17</sup> Additionally, the *SYNE1* gene was frequently methylated in lung cancer cell lines, lung adenocarcinoma, and colorectal cancer.<sup>18,19</sup> By bioinformatic analysis of data from a collection of cancer genome samples, Mascia and Karchin identified *SYNE1* as one of the genes that participated in glioblastoma progression.<sup>20</sup> They observed that mutations in *SYNE1* were associated with a large number of differentially expressed genes.

A role of Nesprin-1 in DNA damage response and DNA repair pathways, which are determinants of genetic instability in cancer and age-associated diseases, has not been investigated. In this report, we analyzed the presence and distribution of Nesprin-1 and associated proteins in cancer cell lines and studied the consequences of a loss of Nesprin-1 in knockdown cells. We further identified components of the DNA damage response (DDR) and DNA mismatch repair (MMR) pathways

\*Correspondence to: Angelika A Noegel; Email: noegel@uni-koeln.de

Submitted: 11/29/2013; Revised: 04/24/2014; Accepted: 04/25/2014; Published Online: 04/29/2014

<http://dx.doi.org/10.4161/nucl.29023>

as binding partners of Nesprin-1. Alterations in the genetic stability upon loss of Nesprin-1 were accompanied by defects in nucleus morphology, centrosome positioning, and nuclear membrane structure, which suggest functions for Nesprin-1 in the maintenance of genome stability. We propose that Nesprin-1 is required for the correct functioning of proteins that have roles in DNA repair.

## Results

### Nesprin-1 isoform expression in cancer cell lines

As mutations in *SYNE1* have been identified in different types of human cancers and Nesprin-1 transcripts were downregulated at early tumor stages in a wide range of human carcinomas ([www.oncomine.org](http://www.oncomine.org)),<sup>15</sup> we probed several cancer cell lines both from human and mouse with Nesprin-1 specific antibodies by immunoblotting and immunofluorescence. Monoclonal antibody K43-322-2 generated against spectrin repeats 9, 10, and 11 (Fig. 1A) recognized proteins of ~600, 400, 300, 250, 150, 55, and 50 kDa in CH310T1/2 cells. The proteins correspond in their molecular weights to Nesprin-1 isoforms described in a recent detailed analysis.<sup>21</sup> The ~600 and 400 kDa proteins were absent from all cancer cell lines and only the ~150 kDa protein was present with the exception of WIDR, where ~300, 250, 150, and 60 kDa proteins were detected. In the CT26 and Huh7 cell lysates the signal was rather faint, even after prolonged exposure (Fig. 1B, and data not shown). Furthermore, a protein of high molecular weight, which presumably corresponds to Nesprin-1 Giant<sup>22</sup>, was detected in C2F3, HaCaT, and HeLa and Hep3B cell lysates. Based on the low expression levels of the N-terminal Nesprin-1 isoforms in Hep3B and Huh7 liver cancer cells compared with colon, cervix, and skin cancer cells, we focused our studies on these cell lines. Furthermore, recent data also suggested that Nesprin-1 expression levels are significantly reduced in liver cancer samples compared with matched normal tissue (<http://www.oncomine.org>).

In the following studies, we included THLE-2 cells. They are immortalized human hepatocyte cells and should reflect the situation in the non-cancer state. Nesprin-1 C-terminal isoforms were identified in THLE-2, Hep3B, and Huh7 cell lysates with polyclonal SpecII antibodies directed against the C-terminus of Nesprin-1.<sup>23</sup> In THLE-2 cells we detected ~600 and 400 kDa proteins which were absent from Hep3B and Huh7. Instead, they harbored low levels of ~150 and 100 kDa and in case of Hep3B of ~300 and 250 kDa proteins (Fig. 1C). We also probed murine skin and liver tissues and observed that they expressed significant levels of Nesprin-1 (Fig. S1A and B). In further studies we compared Nesprin-1 expression in lysates from normal mammary tissue (N1, N2, and N3) and tumor tissue (T1, T2, and T3) of different patients. The SpecII antibodies recognized primarily a ~55 kDa protein which was strongly reduced in the tumor tissue (Fig. S1C and D). When probing for Nesprin-2, we detected isoforms of Nesprin-2 with polyclonal antibodies pAbK1 directed against the C-terminus of Nesprin-2. The amounts were higher in THLE-2 cells as compared with Hep3B and Huh7 cells (Fig. 1D).

### Hep3B and Huh7 have nuclear shape defects and alterations in components of the nuclear envelope

The nuclei of Hep3B and Huh7 cells were enlarged and often displayed a deformed morphology in contrast to the oval shape in THLE-2 cells. We further noted folds, lobulations, protrusions, blebs, and micronuclei (Fig. 2A). In Hep3B, 37% of the cells had misshapen nuclei, in Huh7 26% and in the THLE-2 control 16%. Micronuclei were observed in 11% of the Hep3B cells, in 8% in case of Huh7, and 4% of THLE-2 cells (Fig. 2B; bar graph). SpecII antibodies labeled the NE in THLE-2 cells and gave some cytoplasmic staining in the vicinity of the nucleus whereas the Nesprin-1 presence at the NE was strongly reduced in the cancer cells (Fig. 2A). Remarkably, Emerin was nearly completely absent from the NE in the liver cancer cells (Fig. 2A and B; bottom panel). The absence of Emerin was also confirmed in western blots (Fig. 1C). By contrast, in colon cancer cell lines Nesprin-1 and Emerin localization was unperturbed (Fig. S1E). Lamin A/C specific antibodies showed a rim-like staining pattern in THLE-2. In Hep3B and Huh7 cells a discontinuous, patchy Lamin A/C distribution at the NE was observed. Lamin B1 staining of the NE was homogenous in THLE-2 cells, in Hep3B and Huh7 cells the distribution was patchy (Fig. 2C; arrow heads). LAP2, a member of a group of NE proteins involved in tethering chromatin to the nuclear envelope<sup>24</sup> and affecting gene expression,<sup>25</sup> showed an unaltered localization at the NE in Hep3B and Huh7 cells (Fig. 2C). The expression level was higher in Hep3B and Huh7 cells than in THLE-2 cells which expressed low amounts of LAP2 (Fig. 1C).

NPC proteins regulate nuclear transport, are connected to chromatin and participate in the regulation of transcription.<sup>26,27</sup> Increased expression of individual NPC components has been noticed in several tumor types.<sup>17,28–33</sup> Hep3B and Huh7 cells exhibited NE staining with mAb 414, which recognizes several NPC proteins based on the presence of FXFG-repeats, however staining was reduced in nearly 45% of the cells (Fig. 2D and E). Analyzing individual proteins by western blotting we found that NUP153 levels were higher in Hep3B and Huh7 cells compared with the THLE-2 and NUP116 levels were decreased. The expression level of NUP62 was not altered in Hep3B and Huh7 cells (Fig. 1D).

Immunofluorescence analysis for SUN proteins revealed a rim like staining for SUN1 in THLE-2, Hep3B and Huh7 cells. Some cells exhibited a brighter SUN1 staining which was associated with misshapen and enlarged nuclei (Fig. 2F and G, arrow heads). Quantification of the cells with strong SUN1 staining showed that SUN1 was significantly increased in Hep3B, Huh7 cells as compared with THLE-2 (Fig. 2H). When we examined the amounts of SUN1 and SUN2 in western blots we found that particularly the SUN1 levels were higher in Hep3B and Huh7 as compared with THLE-2 (Fig. 1C; Fig. S2A).

### The centrosome-nucleus distance is increased in Hep3B and Huh7 cells

Centrosomal aberrations are frequently observed in cancer cells. Normal cells in the G1 phase of the cell cycle have a single centrosome that is attached to the nucleus. In THLE-2 cells, centrosomes were positioned near the nucleus at a mean

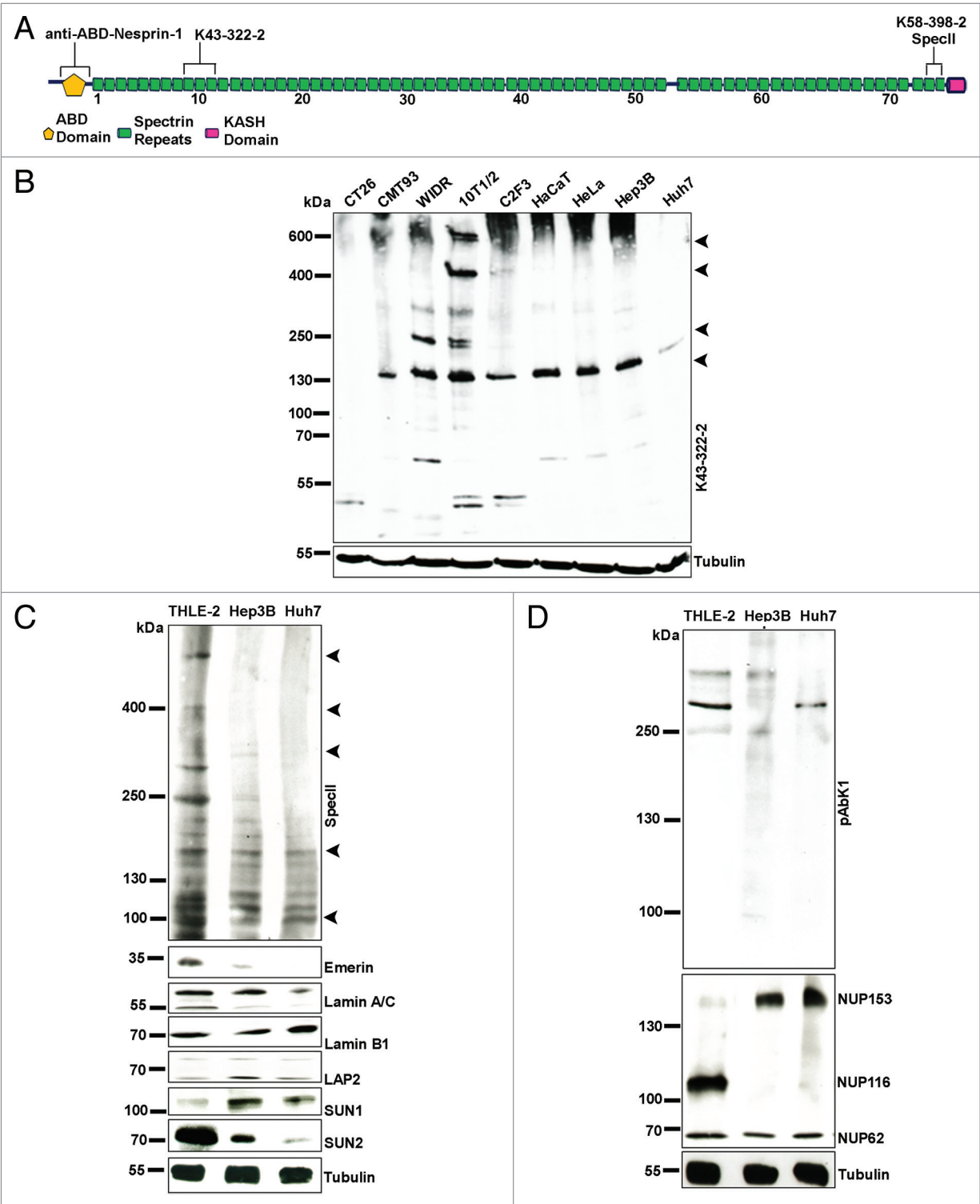


**Figure 1.** Nesprin-1 isoforms in various cell lines. **(A)** Location of the binding sites of Nesprin-1 antibodies. The largest isoform Nesprin-1 Giant is depicted. ABD, actin binding domain. **(B)** Lysates of the indicated cell lines were separated on a 3–15% SDS-PA gradient gel and probed with mAb K43-322-2 to detect N-terminal isoforms. Arrow heads point to proteins discussed in the main text. **(C)** Nesprin-1 expression in THLE-2, Hep3B, and Huh7 cells using anti-Nesprin-1 Specll directed against the C-terminus. The blots were probed with Emerin, Lamin A/C, Lamin B1, LAP2, SUN1, and SUN2 antibodies. Tubulin was used to assess equal loading. For **(B)**, tubulin amounts were checked on a separate gel. **(D)** Presence of Nesprin-2 as detected with pAbK1 directed against the C-terminus. NPC proteins were detected with mAb414.

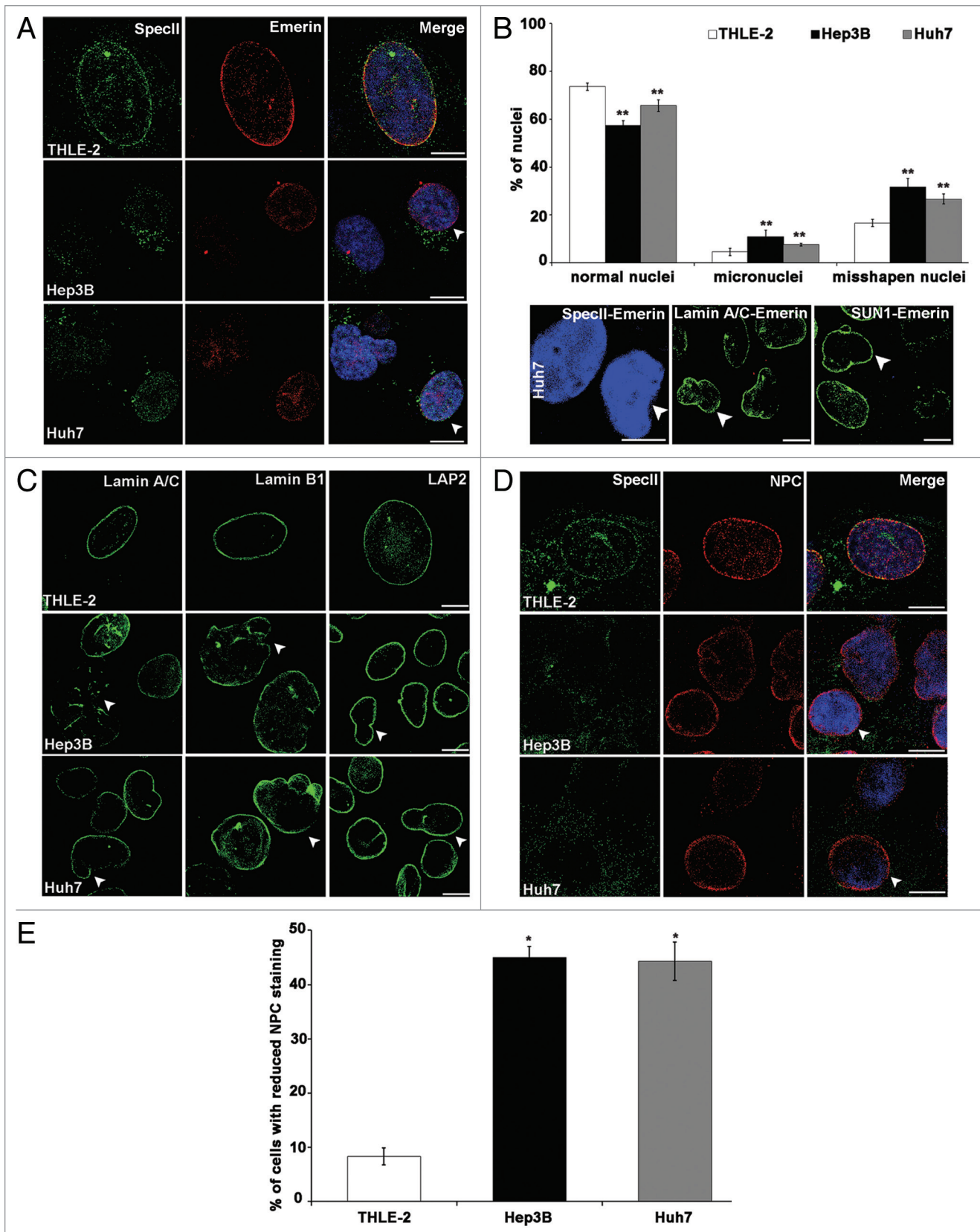


**Figure 2.** For figure legend, see page 178.

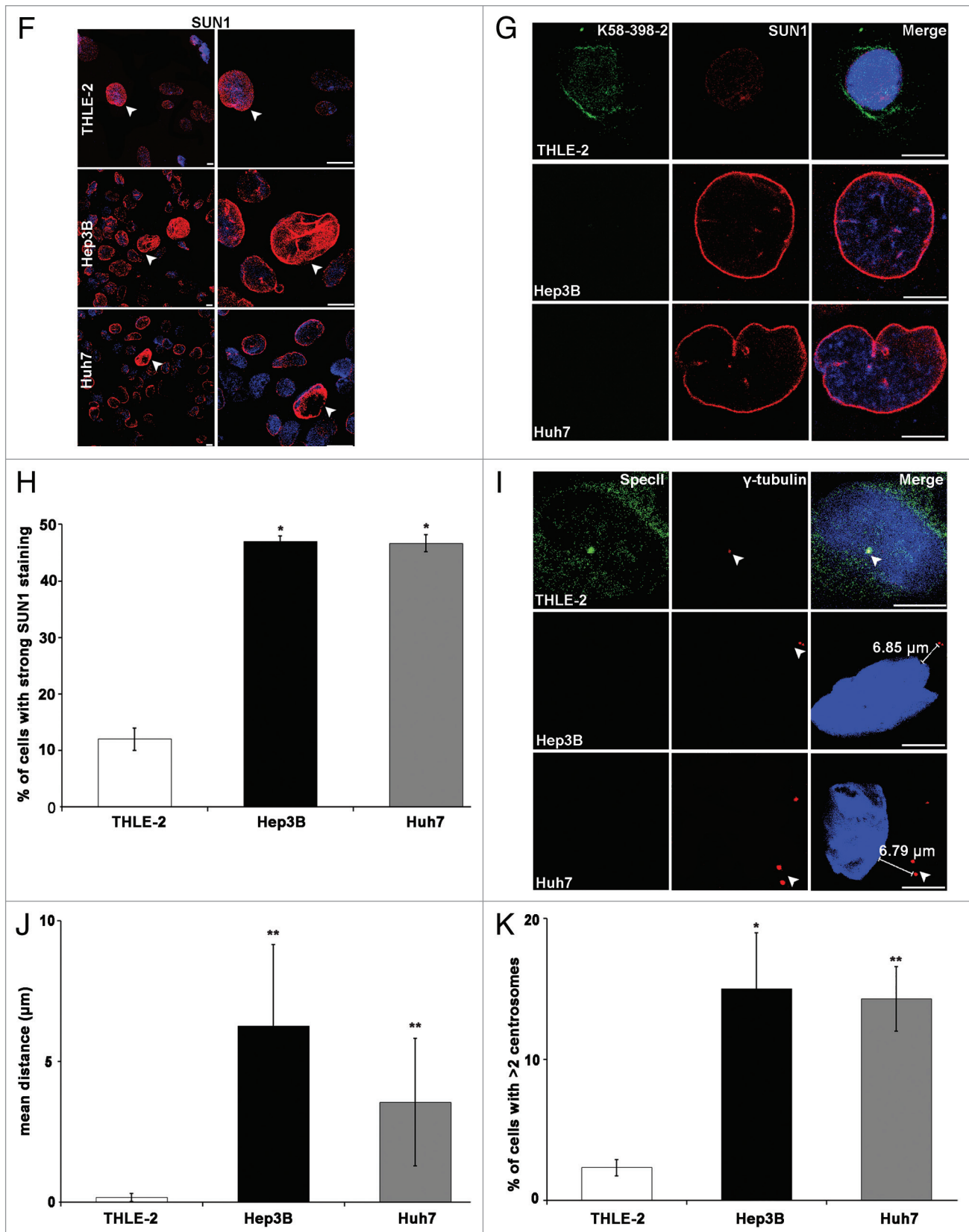


**Figure 2.** For figure legend, see page 178.

**Figure 2 (See previous pages).** Hep3B and Huh7 have nuclear shape defects and alterations in components of the nuclear envelope. **(A)** Staining was with SpecII (green) to detect Nesprin-1 and a mAb specific for Emerin (red). DAPI staining of DNA is in blue. Arrow heads indicate nuclei with regular shape and staining for SpecII and Emerin. Scale bar, 10  $\mu\text{m}$ . **(B)** Huh7 cells have nuclear shape defects and alterations in components of the nuclear envelope. Staining was with polyclonal SpecII antibodies against Nesprin-1 (green), Lamin A/C (green), SUN1 (green), and mAb Emerin (red) antibodies. DAPI staining of DNA is in blue. Scale bar, 10  $\mu\text{m}$ . Upper panel, statistical analysis of nuclear aberrations. 300 nuclei each for THLE-2, Hep3B and Huh7 were evaluated (\*\* $P < 0.0001$ ). **(C)** Distribution of Lamin A/C, Lamin B1, and LAP2 in THLE-2, Hep3B, and Huh7 cells. Arrow heads indicate the observed defects. Scale bar, 10  $\mu\text{m}$ . **(D)** THLE-2, Hep3B, and Huh7 cells were stained with anti-Nesprin-1 SpecII (green), mAb NPC (red), and DAPI (blue). Arrow heads point to normal shaped nuclei stained with SpecII and NPC. Scale bar, 10  $\mu\text{m}$ . **(E)** Statistical analysis of NPC staining. 300 cells per strain were analyzed (\* $P < 0.0001$ ). **(F)** SUN1 (red) staining in THLE-2, Hep3B and Huh7 cells, DAPI, blue. Arrow heads point to cells with high SUN1 expression and misshapen and enlarged nuclei. Scale bar, 10  $\mu\text{m}$ . **(G)** Nesprin-1 (mAb K58–398–2, green) and SUN1 (red) staining in THLE-2, Hep3B, and Huh7 cells. Nuclei are stained with DAPI (blue). Scale bar, 10  $\mu\text{m}$ . **(H)** Statistical analysis of strong SUN1 staining. 300 cells per strain were analyzed (\* $P < 0.0001$ ). **(I)** Centrosome-nucleus-distance is altered in Hep3B and Huh7 cells.  $\gamma$ -Tubulin (red) specific antibodies were used to label the centrosome. DAPI (blue), nuclear staining. Scale bar, 10  $\mu\text{m}$ . **(J)** Statistical evaluation of the centrosome-nucleus distance. **(K)** Statistical evaluation of cells with  $> 2$  centrosomes. Error bars indicate standard deviations (\* $P < 0.001$ , \*\* $P < 0.0001$ ).

distance of  $0.17 \pm 0.15 \mu\text{m}$ . In Hep3B and Huh7 cells, the distance between the centrosome and the nucleus was highly variable, and cells with normal shaped as well as deformed nuclei displayed an increased centrosome-nucleus distance. In Hep3B and Huh7 cells, we observed an increase to  $6.29 \pm 4.24 \mu\text{m}$  and  $3.56 \pm 3.0 \mu\text{m}$ , respectively (Fig. 2I and J). The number of centrosomes also differed; 15% of Hep3B and 14.3% of Huh7 cells had more than two centrosomes (Fig. 2K). The centrosome number was not necessarily associated with nuclear shape changes.

#### Knockdown of Nesprin-1 elicits changes that are observed in cancer cell lines

To test whether a loss of Nesprin-1 can cause the changes observed in the cancer cells, we reduced the amounts of Nesprin-1 by shRNA mediated knock down in CH310T1/2 (KD-CH310T1/2) and in human fibroblasts (KD-HF) using knockdown vectors targeting N-terminal and C-terminal sequences and analyzed the consequences. For control we used untransfected cells (HF, CH310T1/2) and cells transfected with the empty pSHAG-1 vector (C-HF, C-CH310T1/2). Western blot analysis with mAb K43-322-2 and SpecII labeling confirmed the knock down (Fig. 3A and B). Labeling with mAb K43-322-2 showed that in Nesprin-1 KD cells particularly the 250 kDa and larger proteins of 400 and 600 kDa were significantly reduced in amounts (Fig. 3A; arrow heads). The 130 kDa protein and smaller proteins were also less prominent. The expression level of the smallest ones were not altered as was the level of a  $\sim 200$  kDa protein (Figure 3A). The identity of this protein is unclear as such an isoform has not been reported. The transcript levels were also significantly reduced (Fig. S2B; shown for fibroblasts). Reduction of Nesprin-1 was associated with a downregulation of Emerin, Lamin B1, NPC proteins and LAP2. By contrast, SUN1 and SUN2 protein amounts were increased (Fig. 3A; Fig. S2C). This was also observed for SUN1 in CH310T1/2, in which the levels of endogenous SUN1 were quite low (Fig. 3A and E).

In immunofluorescence analysis, the clear NE staining by SpecII and Emerin antibodies was lost, and some residual punctate staining in the cytosol was seen in the knockdown cells. Similar results were obtained for the NPC antibodies (Fig. 3C and D; Fig. S3A and B). Nearly all cells that had an altered staining pattern exhibited nuclear shape defects. SUN1 antibodies strongly stained the NE in KD-HF. Cells with particularly strong SUN1 staining exhibited a variety of nuclear shape defects including folds, lobulations, blebs, and micronuclei (Fig. 3E).

Quantification of the mRNA levels by qRT-PCR showed that SUN1 and SUN2 mRNA were significantly increased in KD-HF cells as compared with HF (Fig. S3C). Furthermore, Nesprin-1 knockdown fibroblasts, Hep3B, and Huh7 cells exhibited increased nuclear deformations with folds and pleats after heat treatment (Fig. S3D and E). Many nuclei also displayed notches, tears, and herniations (Fig. S3D; arrow heads). Knockdown with plasmids targeting N-terminal or C-terminal sequences showed similar results as knockdown experiments where we used vectors targeting N-terminal and C-terminal sequences together.

#### The centrosome-nucleus distance is increased in Nesprin-1 KD cells

We investigated the centrosome-nucleus distance and centrosome number upon loss of Nesprin-1 and found that centrosomes were positioned  $0.35 \pm 0.29$  and  $3.20 \pm 2.34 \mu\text{m}$  away from the NE in C-HF and Nesprin-1 KD-HF cells, respectively. Similarly, the mean centrosome-nucleus distance increased from  $0.44 \pm 0.27 \mu\text{m}$  in C-CH310T1/2 cells to  $2.40 \pm 1.49 \mu\text{m}$  in Nesprin-1 KD-CH310T1/2 cells (Fig. 3F and G). Nesprin-1 loss was also accompanied by alterations of the centrosome number. More than two centrosomes were seen in 3.3% C-HF; for Nesprin-1 KD-HF this number increased to 10%, and for CH310T1/2 it increased from 6% in the C-CH310T1/2 to 11% after knockdown (Fig. 3H).

#### The actin-binding domain (ABD) of Nesprin-1 interacts with DNA mismatch repair proteins MSH2 and MSH6

Nesprin-1 harbors an F-actin binding domain (ABD) at its N-terminus. In a search for Nesprin-1 interaction partners, we performed pull-down experiments with GST-Nesprin-1-286 encompassing the ABD and C2F3 cell lysates. Among the identified proteins was the DNA mismatch repair and damage recognition protein MSH2. This reaction was specific and GST-Nesprin-1-286 did not bind to DNA damage proteins in general, as, i.e., the p53 protein did not interact (data not shown). To verify the interaction we repeated the experiment with HeLa cell lysates and probed the precipitate directly for the presence of MSH2 with antibodies. We also found MSH6 in the precipitate. MSH2 forms a complex with MSH6 (MutS $\alpha$ ) which binds to DNA mismatches and functions in the repair of DNA double strand breaks.<sup>34</sup> GST alone as control did not precipitate MSH2 and MSH6 (Fig. 4A). To probe the interaction of Nesprin-1 with MSH2 and MSH6 in vivo, we transiently expressed GFP-Nesprin-1-286 in COS7 cells. GFP-Nesprin-1-286

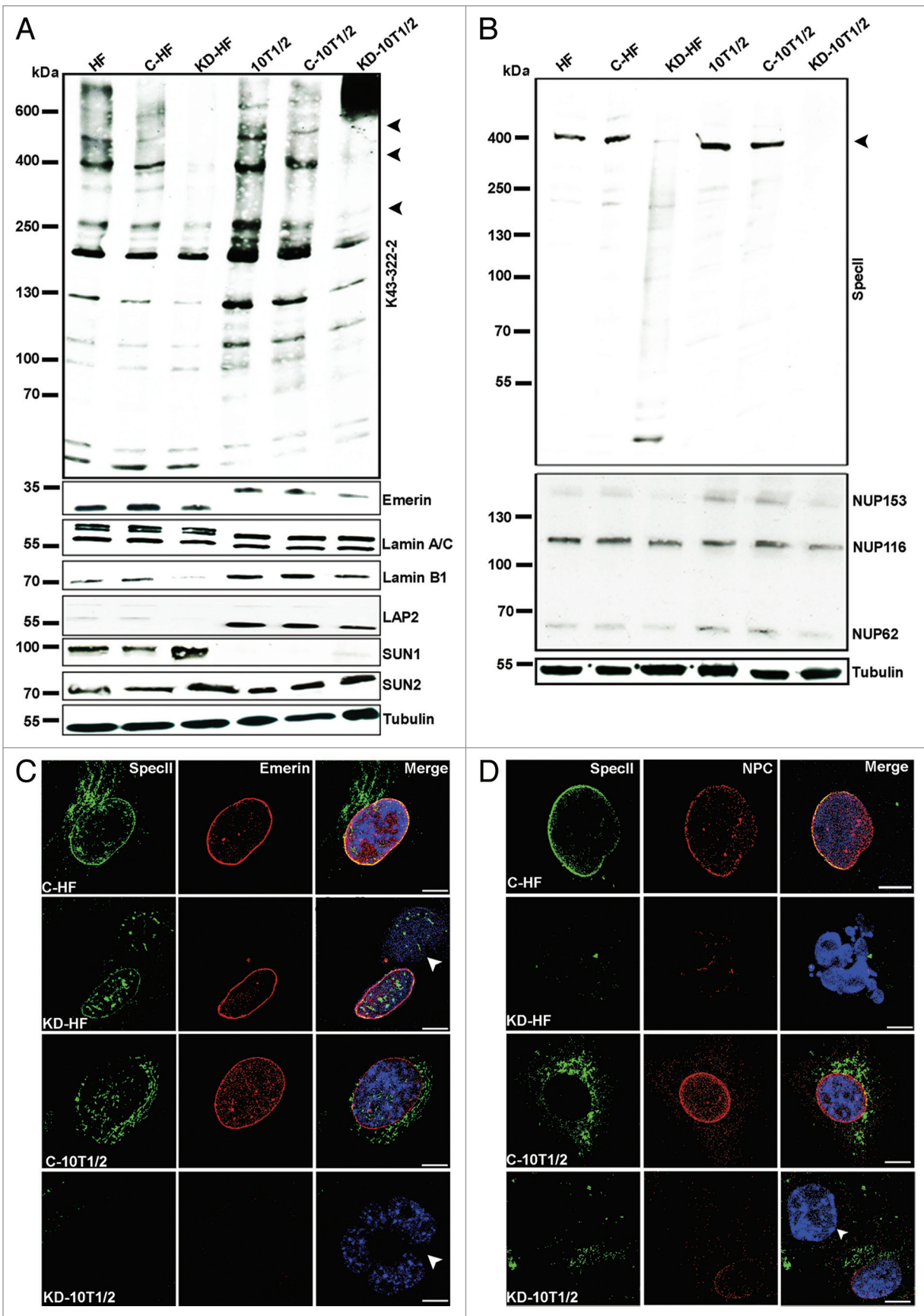


**Figure 3.** For figure legend, see page 181.

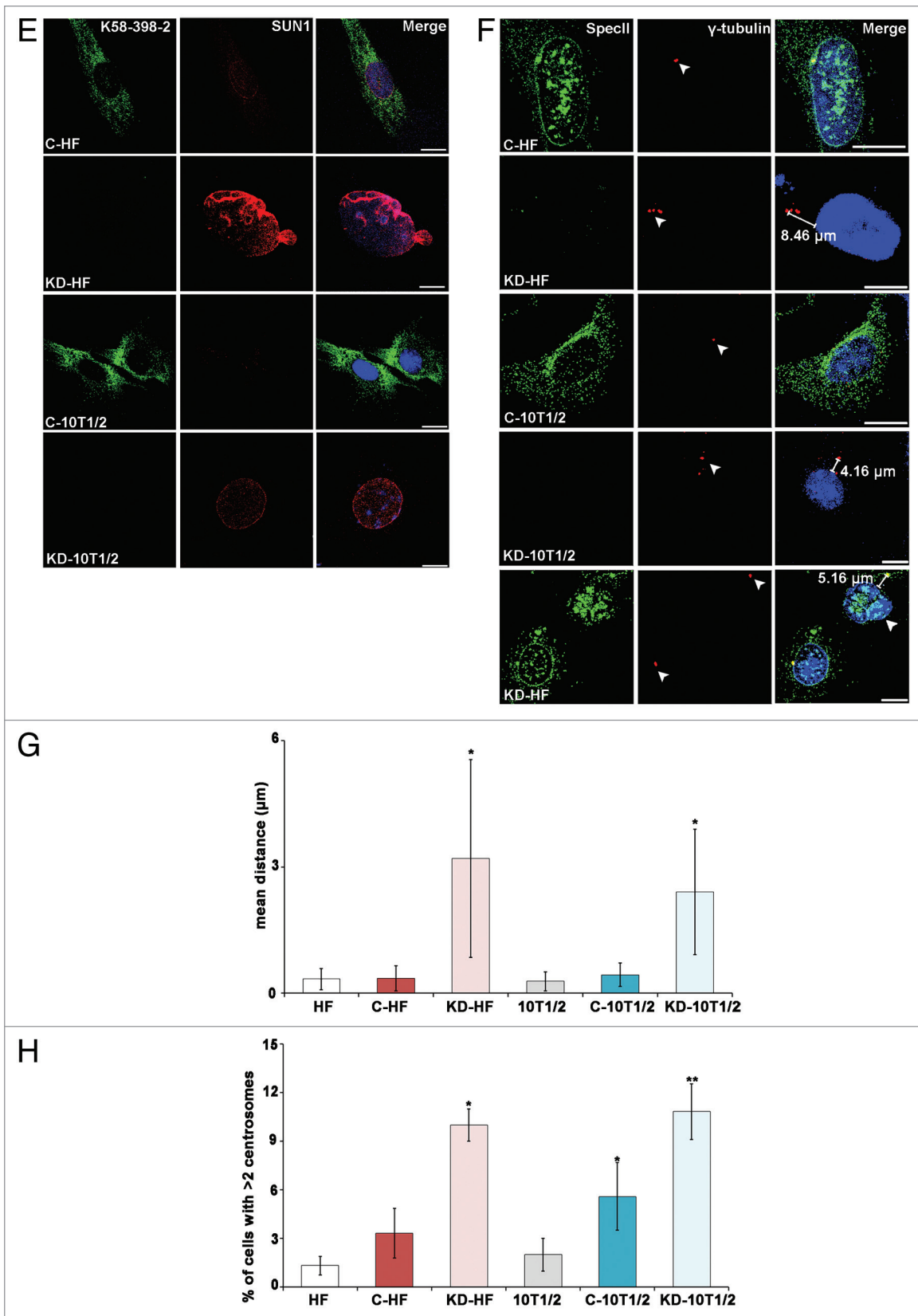


**Figure 3.** For figure legend, see page 181.

**Figure 3 (See previous pages).** Knock down of Nesprin-1 elicits alterations that are observed in cancer cell lines. **(A, B)** Immunoblot analysis of Nesprin-1 knock down HF and CH310T1/2 cells. Detection was with mAb K43–322–2 and pAb SpecCl. Tubulin served as control. Emerin, Lamin A/C, Lamin B1, LAP2, SUN1, and SUN2 specific antibodies were used for analysis. Human and murine Emerin differ in their primary sequence explaining the observed difference in molecular weight. The blot in A was reprobed with SpecCl antibodies and mAb414 to detect NPC proteins **(B)**. **(C, D)** Effect of Nesprin-1 knock down on NE components. Cells were stained for Nesprin-1 with pAb SpecCl (green), Emerin (red), mAb NPC (red), and DAPI (blue). Arrow heads indicate the NE phenotypes described. Scale bars, 10  $\mu$ m. **(E)** SUN1 (red) staining in C-HF, KD-HF, C-CH310T1/2, KD-CH310T1/2 cells. Nesprin-1 was detected with mAb K58–398–2 (green). Nuclei are stained by DAPI (blue). **(F)** Centrosome position in C-HF, KD-HF, C-CH310T1/2, and KD-CH310T1/2 cells. Centrosomes were visualized with a  $\gamma$ -tubulin antibody (red), Nesprin-1 with SpecCl (green). The nucleus was stained with DAPI (blue). Scale bars, 10  $\mu$ m. **(G)** Statistical evaluation of the centrosome-nucleus distance. 100 cells for each cell line were evaluated (\* $P < 0.0001$ ). **(H)** Statistical analysis of the percentage of cells with  $>2$  centrosomes was calculated from three independent experiments (100 cells were counted per experiment, \* $P < 0.05$ , \*\* $P < 0.0001$ ).

colocalized with MSH2 and MSH6 at the nuclear envelope and also inside the nucleus (Fig. 4B). We then performed immunoprecipitation experiments. GFP-Nesprin-1-286 was immunoprecipitated from nuclear extracts using GFP beads, and the precipitates were probed for the presence of MSH2 and MSH6. We found that MSH2 and MSH6 coprecipitated with GFP-Nesprin-1-286 (Fig. 4C). To address the question of whether the interaction of Nesprin-1-286 with MSH2 and MSH6 is direct, we performed blot-overlay assays. A membrane containing HF lysate was overlaid with GST-Nesprin-1-286. GST signals were detected at the correct size of MSH2 and MSH6 that had been revealed by staining with MSH2 and MSH6 antibodies (Fig. 4D). Moreover, we immunoprecipitated GFP-Nesprin-1-286 and GFP from COS7 cells, separated them by SDS-PAGE, transferred the proteins to nitrocellulose membranes, and performed overlay assays with a fusion protein that consisted of GST and N-terminal sequences of MSH2, GST-MSH2-1-138, or GST. GST-MSH2-1-138 bound to Nesprin-1-286, whereas GST did not (Fig. 4E).

Next we tested whether MSH2 and MSH6 levels were affected by Nesprin-1 levels. By protein analysis we found that Huh7 and KD-HF cells expressed low levels of MSH2 and nearly no MSH6 was seen, whereas their levels were considerably higher in Hep3B and HF (Fig. 4F). In agreement, in Huh7 and KD-HF cells the amounts of Nesprin-1 detected with anti-ABD-Nesprin-1 were much lower compared with Hep3B and HF cells, as were the transcript levels (Fig. 4G; Fig. S2B). We also included the human colorectal cell line DLD-1, which is deficient in DNA mismatch repair, to test whether its deficiency correlates with the Nesprin-1 levels. In western blots we found low levels of MSH2 and nearly no MSH6 (Fig. 4F), and with ABD-Nesprin-1 antibodies we detected only the ~100 kDa protein in reduced amounts. Interestingly, it was recently reported that SYNE-1 is a candidate gene for colorectal cancer, but the molecular mechanism was not elucidated.<sup>17</sup> DLD-1 cells also showed abnormal nuclear morphology, centrosomal aberrations, and altered expression of NE components as were observed in Nesprin-1 KD cells (Fig. S4A). Furthermore, we observed reduced expression of MSH2 and fewer MSH6 foci in KD-HF cells compared with C-HF cells (Fig. 5A and B). Quantification of the MSH2 and MSH6 mRNA levels by qRT-PCR showed that they were significantly reduced in Nesprin-1 KD-HF cells. Similar results were obtained with KD-HeLa cells (Fig. 5C).

In order to determine possible effects of Nesprin-1 on the MSH2-MSH6 heterodimer during DNA replication or repair process, C-HF and KD-HF cells were synchronized at G1, S,

or G2/M phases and the chromatin association of the proteins tested. The cell cycle status was confirmed by flow cytometry (FACS). Colocalization of Nesprin-1 with MSH2 and MSH6 was observed in S phase (Fig. 5D and E). Notably, the Nesprin-1 positive HF cells expressed high levels of MSH2 and MSH6 during S phase. Nesprin-1 deficient cells had strongly reduced levels of MSH2; MSH6 was undetectable (Fig. 5D and E; Fig. S4B and C). We propose that localization of MSH2-MSH6 to the nucleus and to chromatin is facilitated by Nesprin-1 leading to successful DNA repair.

Recent work by Li and coworkers<sup>35</sup> showed that H3K36me3 has a role in MMR and is required to recruit hMSH2-hMSH6 to chromatin. We therefore tested for H3K36me3 presence in early S phase and observed that KD-HF cells behaved like Nesprin-1 positive cells and showed H3K36me3 positive spots (Fig. S4D). H3K36me3 recruitment does therefore not depend on the presence of Nesprin-1 and a later step is affected in KD-HF.

Earlier reports indicated that cell lines defective in MMR exhibit an increased sensitivity to Etoposide.<sup>36–38</sup> Etoposide causes errors during DNA synthesis and has a measurable effect on the mutation rate.<sup>38</sup> In our experiments, the range of Etoposide concentration which inhibited cell growth by 50% (IC<sub>50</sub>) was highest in the C-HF cells (IC<sub>50</sub>, 66  $\mu$ M). By contrast, the KD-HF and DLD-1 cells deficient in Nesprin-1 were highly sensitive to the cytotoxic effects of Etoposide with values of 18.34  $\mu$ M and 3.09  $\mu$ M, respectively (Fig. 5F). These findings strongly suggest that disruption of Nesprin-1 has an impact on the ability of cells to perform MMR.

Nesprin-1 may have an important role for the function of MSH2 and MSH6 to repair mismatches, and a defect in this connection may also lead to alterations in earlier DDR events. Therefore, it is possible that the Nesprin-1 interaction with the MutS $\alpha$  complex is a constitutive cellular event required for proper DNA repair, and the interaction is not required for just the NE localization of the MutS $\alpha$  complex.

#### Loss of Nesprin-1 affects the DNA damage response network

The DDR pathway is associated with cancer development. MMR and non-homologous end joining (NHEJ) repair are two interlinked processes, and loss of MSH2 and MSH6 has been correlated with altered response to double strand breaks (DSBs) as well.<sup>39,40</sup> To gain insight into specific steps during DDR, we monitored the cellular levels of key components, namely histone H2AX, checkpoint kinases Chk1 and Chk2, and Ku70 in THLE-2, Hep3B, Huh7, C-HF, and Nesprin-1 KD-HF cells. Phosphorylation of H2AX, Chk1, and Chk2 is among the initial events that occur in response to DNA damage.<sup>41–43</sup> Ku70/

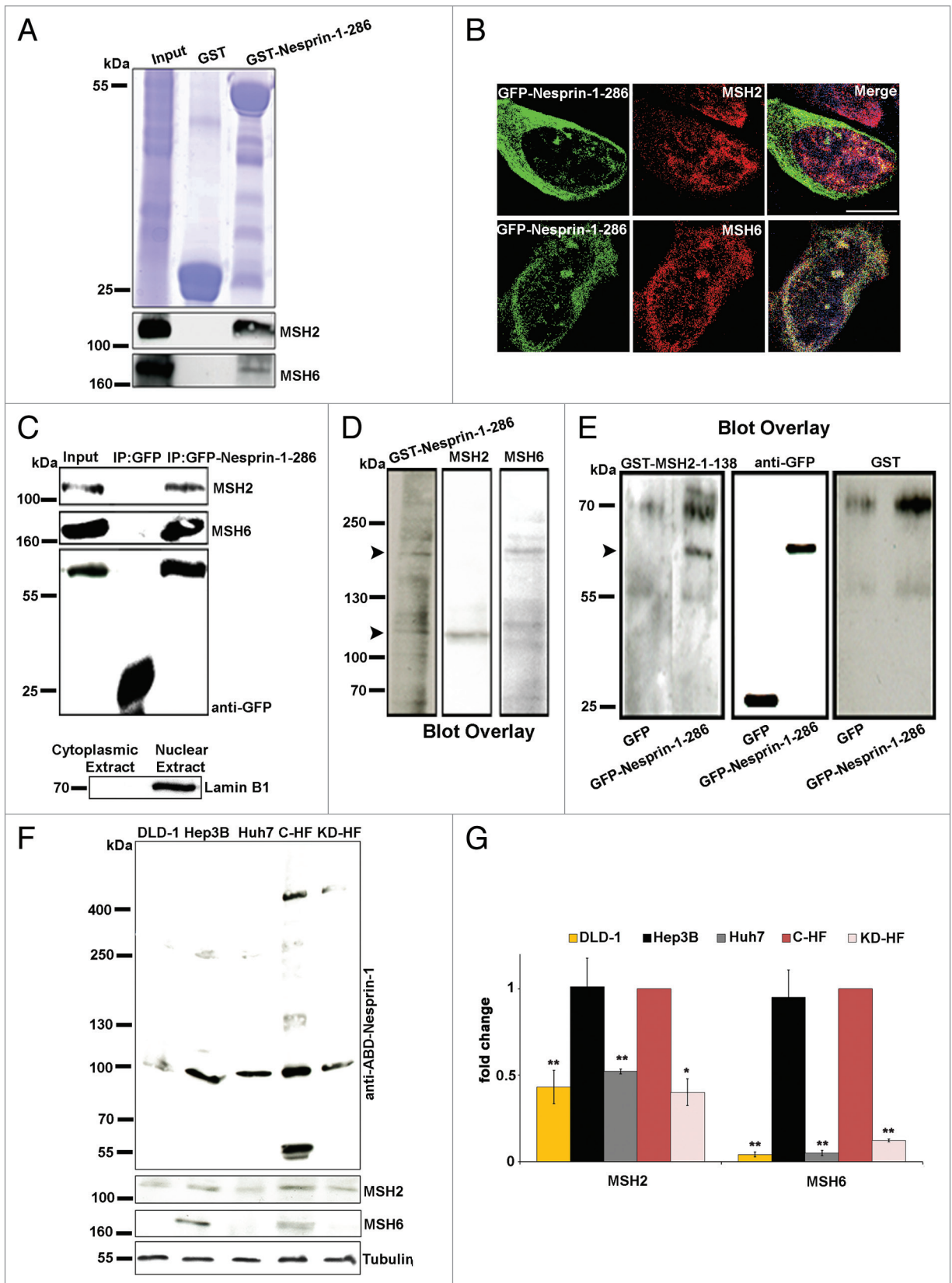


**Figure 4.** For figure legend, see page 183.

**Figure 4 (See opposite page).** Nesprin-1 interacts with MMR proteins. **(A)** Interaction of Nesprin-1 with MSH2 and MSH6. HeLa cells were incubated with GST-Nesprin-1-286 and GST for control. Detection of the 105 kDa MSH2 and 163 kDa MSH6 in the pull down was with MSH2 and MSH6 specific antibodies, respectively (lower panels). Upper panel, Coomassie Blue staining of the gel. **(B)** COS-7 cells were transfected with GFP-Nesprin-1-286 (green) and stained with MSH2 (red) and MSH6 (red). Scale bar, 10  $\mu$ m. **(C)** Interaction of GFP-Nesprin-1-286 with MSH2 and MSH6 in nuclear extract as revealed by coimmunoprecipitation. GFP-Nesprin-1-286 and GFP were detected with mAbs specific for GFP. Subcellular fractionation (nuclear and cytoplasmic extract) was confirmed with Lamin B1 specific antibodies (lower panel). **(D)** Blot overlay showing that Nesprin-1-286 binds MSH2 and MSH6 directly. HF cell lysate containing membrane was overlaid with GST-Nesprin-1-286 (left panel). In the middle panel the membrane was probed with MSH2 specific antibodies, the right panel was probed with MSH6 specific antibodies to reveal the location of the proteins. The arrows on the left indicate the location of MSH2 and MSH6. **(E)** The membranes with immunoprecipitated GFP-Nesprin-1-286 and GFP were overlaid with GST-MSH2-1-138 (left panel) or GST for control (right panel). Binding was detected by subsequent incubations with anti-GST polyclonal antibodies. Blots were incubated with anti-GFP mAb to reveal the location of GFP and GFP fusion protein (middle panel). The arrow points to GFP-ABD-Nesprin-1. GST reacted with ~55 and 70 kDa proteins. **(F)** Immunoblot analysis of DLD-1, Hep3B, Huh7, C-HF, and KD-HF cells for Nesprin-1 detected with anti-ABD-Nesprin-1, MSH2, and MSH6. Tubulin served as control. **(G)** Histograms representing fold changes of band intensities of MSH2 and MSH6. Band intensities were normalized relative to the loading control (tubulin). Data are the mean  $\pm$  SD from three samples per group of three independent experiments (\* $P$  < 0.001, \*\* $P$  < 0.0001).

Ku80 binds to DNA double-strand breaks during NHEJ and recruits the DNA-dependent protein kinase catalytic subunit to the lesion. Notably, the Ku70/Ku80 heterodimer protects the broken DNA ends from unwanted or excessive nucleolytic attack which leads to loss of genetic information and unsuccessful DNA repair.<sup>44-46</sup> In THLE-2 and C-HF cells nearly no  $\gamma$ H2AX foci marking broken DNA were observed. Upon HU, UV and Etoposide treatment  $\gamma$ H2AX positive spots formed. After knock down of Nesprin-1 a strong increase in the number of  $\gamma$ H2AX foci was observed that exceeded the one of C-HF cells after HU, UV, or Etoposide treatment and was indicative of an elevated DNA damage upon loss of Nesprin-1 (Fig. 6A-C). Untreated Hep3B and Huh7 cells had a similar high number of  $\gamma$ H2AX foci. This number was further enhanced following HU, UV, and Etoposide treatment both in Nesprin-1 KD and the tumor cells (Fig. 6D; Fig. S5A-E). After HU or UV treatment Ku70 levels decreased in KD-HF cells (Fig. 6E and F). The decrease was also detected at the protein level (Fig. 7A and C). Nesprin-1 reduction also had an effect on the presence of phosphorylated H2AX, Chk1, and Chk2 (Fig. 7B and D-F). In all untreated cell lines, no phosphorylated Chk1 and Chk2 was detected. Upon HU treatment their level strongly increased as detected with antibodies recognizing specific phosphorylated forms in all cell lines except for C-HF where the increase was hardly noticeable (Fig. 7A). The elevated levels of these proteins indicate greater DNA damage in KD-HF compared with C-HF cells (Fig. 7B and D-F). Ku70 was present in untreated Hep3B, Huh7, and C-HF, whereas KD-HF cells had very low levels. Upon HU-treatment the levels decreased in Hep3B, Huh7, and KD-HF. By contrast, an increase was seen in C-HF cells (Fig. 7A and C). A defective response in the tumor cell lines and in Nesprin-1 deficient cells causes a defective recruitment of Ku70 to sites of DNA damage. These findings highlight that Nesprin-1 is required for an efficient NHEJ.

## Discussion

The mechanisms establishing nuclear architecture are not sufficiently known nor are the consequences of a deformed nucleus for normal cell function unraveled. Nuclei of most normal cells have a smooth and ovoid shape, whereas in many cancer cells severe nuclear distortions are observed. We studied

liver cancer cells and found several alterations which we could reproduce by reducing levels of Nesprin-1 by knockdown in several cells.

Most remarkable were the loss of Emerin, an upregulation of SUN proteins and changes in the DDR. It could well be that some of the changes observed in this study are due to Emerin loss or mislocalization. Similarly, Zhang et al. reported that Nesprin-1 siRNA knockdown in fibroblasts affected Emerin localization.<sup>7</sup> This correlated with deformed nuclei. From this, we propose that loss of Nesprin-1 is a casual event in tumorigenesis in analogy to a recent report showing that Emerin reduction was the basis of nuclear morphological deformation and subsequently the cause of aneuploidy in ovarian cancer cells.<sup>47</sup> Whether the deformation of the nuclei is a relevant factor in tumorigenesis is an open question. Deformed nuclei have also been observed upon changes in the LINC complex and in fibroblasts from patients suffering from laminopathies. In these cases the altered shape of the nuclei was not accompanied by enhanced tumorigenesis.<sup>48,49</sup>

Deformed nuclear shape and increased size are also SUN1 dependent. Although the function of SUN1 and SUN2 in cancer biology is undefined, the finding that SUN1 overaccumulation increases nuclear defects in HGPS cells is of great significance.<sup>50</sup> We also noted that brighter SUN1 staining was associated with misshapen and enlarged nuclei in Nesprin-1 KD, Hep3B, and Huh7 cells. Furthermore, Zhang and coworkers found an upregulation of SUN1 and SUN2 in neonatal Nesprin 1<sup>-/-</sup> cardiac and skeletal muscle, respectively.<sup>13</sup>

The response to DNA damage plays a key role in cancer progression and suppression.<sup>51,52</sup> Defects in the DDR network can predispose to cancer and foster cancer progression. To date, the effect of Nesprin-1 deficiency on DNA repair mechanisms has not been addressed. Lei et al. reported a reduction of  $\gamma$ H2AX and phosphorylated Chk1 in Sun1<sup>-/-</sup>Sun2<sup>-/-</sup> mouse embryonic fibroblasts and proposed an impairment of specific pathways.<sup>53</sup> Our results indicated elevated levels of  $\gamma$ H2AX, phosphorylated Chk1 and Chk2 in Nesprin-1 KD-HF, Hep3B, and Huh7 cells pointing toward overactive pathways which can cause chromosomal instability. An integration of Nesprin-1 into the DDR and MMR pathways is further supported by its interaction with components of these pathways in pull down assays. Furthermore, bioinformatic analysis by Mascia and Karchin led to the proposal of an interaction network around Nesprin-1 that contains MSH2 and MSH6.<sup>20</sup> We identified both proteins in

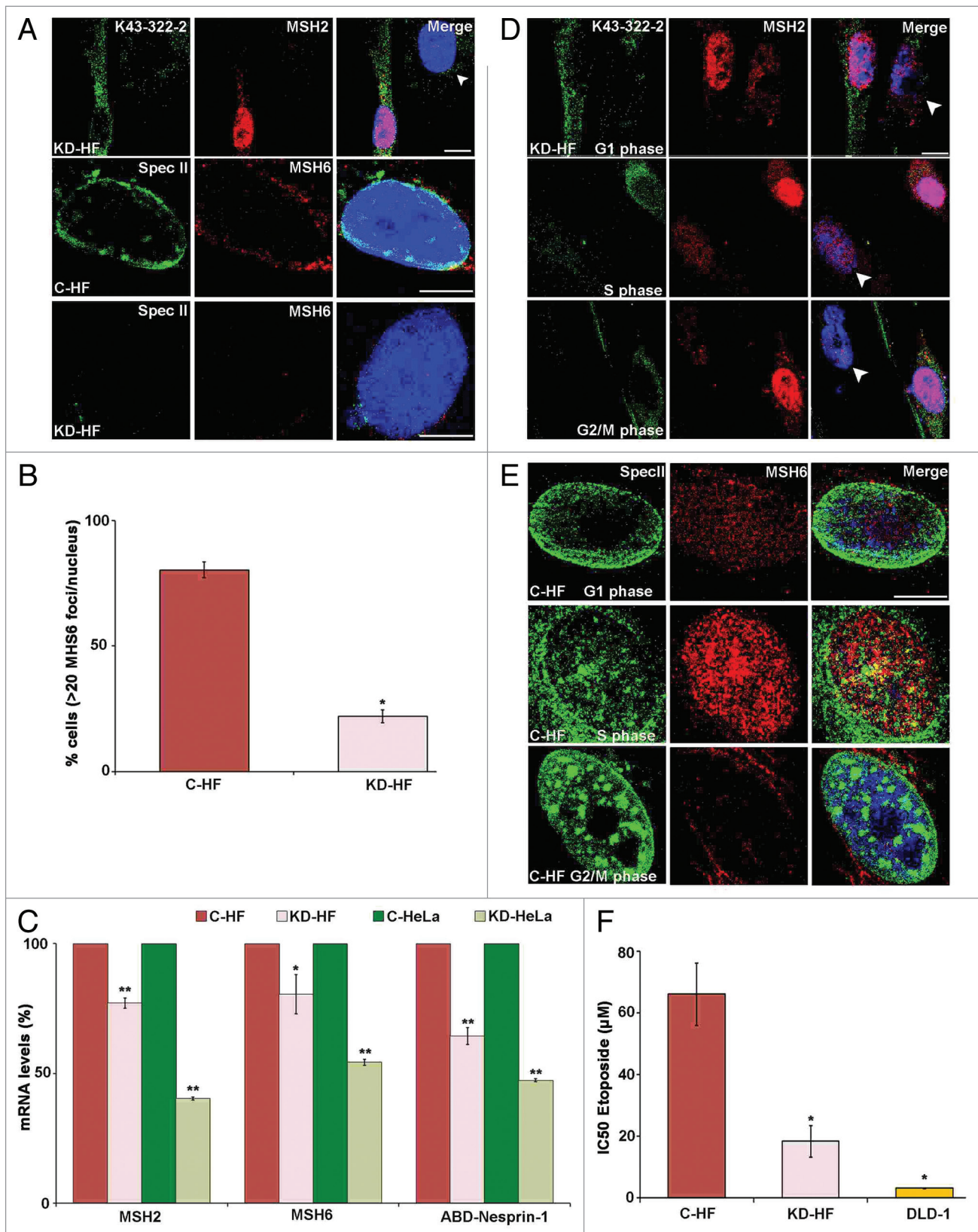


**Figure 5.** For figure legend, see page 185.

pull down experiments using the ABD of Nesprin-1 assigning a role to Nesprin-1 isoforms in the MMR pathway that harbor this domain.

**Figure 5 (See opposite page).** Effect of Nesprin-1 knock down on MSH2 and MSH6. **(A)** Nesprin-1 was detected with K43-322-2 (green) or pAb SpecII (green). MSH2 (red), MSH6 (red), and DAPI (blue). Arrow head indicates the KD-HF cell. Scale bars, 10  $\mu$ m. **(B)** Quantification of the percentage of cells presenting >20 MSH6 foci for C-HF (red bar) or KD-HF (pink bar). Error bars represent standard deviations (\* $P$  < 0.0001). **(C)** MSH2, MSH6 and Nesprin-1 transcript levels in C-HF, KD-HF, C-HeLa, and KD-HeLa as determined by qRT-PCR. Significant downregulation of MSH2 and MSH6 was detected in KD-HF and KD-HeLa cells compared with C-HF and C-HeLa cells (\* $P$  < 0.05, \*\* $P$  < 0.0001). For normalization, GAPDH was used. **(D)** KD-HF cells were arrested at G1, S, G2/M as indicated. Immunofluorescence was performed to determine nuclear distribution of K43-322-2 (green) and its colocalization with MSH2 (red). **(E)** Immunofluorescence analysis showing colocalization of MSH6 with Nesprin-1 in C-HF cells. Nesprin-1 (Spec II) and MSH6 localization for C-HF cells in G1, S or G2/M phase. The colocalization is increased in S phase. Scale bars, 10  $\mu$ m. **(F)** Toxic effect of Etoposide to C-HF, KD-HF, and DLD-1 cells. Histograms represent the mean IC<sub>50</sub> values  $\pm$  SD determined after 5 d of culturing with continuous exposure to Etoposide (\* $P$  < 0.001).

The MMR network serves to maintain genome stability.<sup>54,55</sup> Its importance is highlighted by participating in a cell-cycle checkpoint control system by correcting DNA damage and promoting cell-cycle arrest or triggering apoptosis pathways.<sup>56</sup> Defects in MMR resulted in a greatly increased likelihood of developing certain types of tumors.<sup>57</sup> Depending on the type of DNA damage, loss of MMR might result in increased mutagenesis, loss of cell-cycle control, and resistance to apoptosis.<sup>58</sup> We speculate that Nesprin-1 could provide a platform (Fig. 8) for the association of DNA damage response proteins as well as contribute to the organization of the nuclear envelope to generate specific subcompartments where damaged DNA is sequestered and comes in contact with DNA repair proteins and can be repaired as described for yeast.<sup>59</sup> Functional deficiency of the DDR and the MMR pathway leads to increased genomic instability. Based on an altered DDR network in Nesprin-1 deficient cancer cells, adequate DDR inhibitors might provide promising methods for selective killing of cancerous cells and improve the efficiency of radiotherapy and chemotherapy. Thus, during therapy, cancer cells can be killed by DDR inhibitors whereas the surrounding healthy cells can be saved due to their diminished DDR levels. These results can open many doors for the development of DDR inhibitors in therapy.

Loss of Nesprin-1 triggers an altered cell fate which could lead to tumorigenesis. This could be achieved by altered gene expression, altered genome stability and an altered nuclear structure. Our report highlights changes in nuclear morphology, centrosome positioning, nuclear membrane structure, and DNA damage responses upon loss of Nesprin-1. Careful evaluation of Nesprin-1 levels may therefore provide novel approaches for early disease diagnosis, intervention, and treatment.

## Materials and Methods

### Cell culture and transfections

CMT93 (mouse rectum carcinoma), CT26 (murine colorectal carcinoma), WIDR (human colorectal carcinoma), CH310T1/2 cells (embryonic mouse mesenchymal stem cell line), C2F3 (mouse myoblast), HaCaT (human keratinocyte), HeLa (human cervical carcinoma), Hep3B (human hepatocellular carcinoma), and Huh7 (human hepatocellular carcinoma), DLD-1 (human colorectal carcinoma) cell lines (listed in Table S1) were grown in high glucose Dulbecco's Modified Eagle Medium (DMEM, Sigma) supplemented with 10% FBS, 2 mM glutamine, and 1% penicillin-streptomycin. Primary human dermal fibroblasts

(HFs) were isolated from foreskin and cultured in high glucose DMEM. The immortalized liver cell line THLE-2 (kindly provided by Dr Reena Buurman, Institute of Cell and Molecular Pathology, Hannover Medical School) were cultured as described previously using the BEGM Bullet Kit (Lonza).<sup>60</sup> All cells were grown in a humidified atmosphere containing 5% CO<sub>2</sub>.

Nesprin-1 knock down in HF and CH310T1/2 cells was obtained by plasmid-based shRNA. Oligonucleotides were cloned into pSHAG-1 vector using BseRI and BamHI restriction sites.<sup>61</sup> To knockdown Nesprin-1 in HF cells, two sets of primers were designed by taking 31 nucleotides from each of exon 6 (5'-GGATGAAGCG AATCCATGCT GTGGCTAACA T-3') and 143 (5'-GAAGGAGGTC AGTCGTCATA TCAAGGA ACT G-3') of human *SYNE1*. For Nesprin-1 knock down in CH310T1/2 cells, two sets of primers were designed by taking 31 nucleotides each from exon 5 (5'-GGCTAACATT GGCACCGCAC TCAAATTCCT T-3') and 32 (5'-AGAAGTGGCA GCAGTTTAAT TCTGACCTCA A-3') of murine *SYNE1*. The procedure described in ([http://hannonlab.cshl.edu/protocols/BseRI-BamHI\\_Strategy.pdf](http://hannonlab.cshl.edu/protocols/BseRI-BamHI_Strategy.pdf)) was used for primer design. With these shRNAs the N- and C-terminal regions of human and mouse Nesprin-1, respectively, were targeted and should lead to a loss of most Nesprin-1 isoforms. To knock down Nesprin-1, CH310T1/2 cells were transfected twice at intervals of 4 d using the Amaxa Nucleofector kit V solution (Lonza). For HF cells, Lipofectamine 2000 transfection reagent (Invitrogen) was utilized. Cells analyzed were designated untransfected cells, control knockdowns (C-KD), and knockdowns (KD).

### Immunofluorescence

Nesprin-1 polyclonal antibodies (SpecII) and mAb K58-398-2 directed against the C-terminus of human Nesprin-1, affinity-purified rabbit anti-Nesprin-1 ABD, and mAb K43-322-2 directed against the N-terminus were used.<sup>22</sup> pAbK1 was used to detect Nesprin-2.<sup>6</sup> Immunofluorescence and western blotting were done as described.<sup>23</sup> Antibodies used were specific for Emerin (4G5, Abcam), LAP-2 (BD Transduction Laboratories), Lamin B1 (Abcam), Lamin A/C (StCruz), SUN1 (Abcam), SUN2 (Abcam), mAb414 recognizing nuclear pore complex (NPC) proteins (Abcam), anti-phospho-Ser139 H2AX (Millipore), anti-phospho-Ser317 Chk1 (Cell Signaling), anti-phospho-Ser345 Chk1 (Cell Signaling), anti-phospho-Thr68 Chk2 (Cell Signaling), Ku70, MSH2, MSH6 (all Abcam), and appropriate secondary antibodies conjugated to Alexa 488/568 (Invitrogen). Imaging was done by confocal laser scanning microscopy (Leica TCS-SP5). Images were processed using TCS-SP5 software.

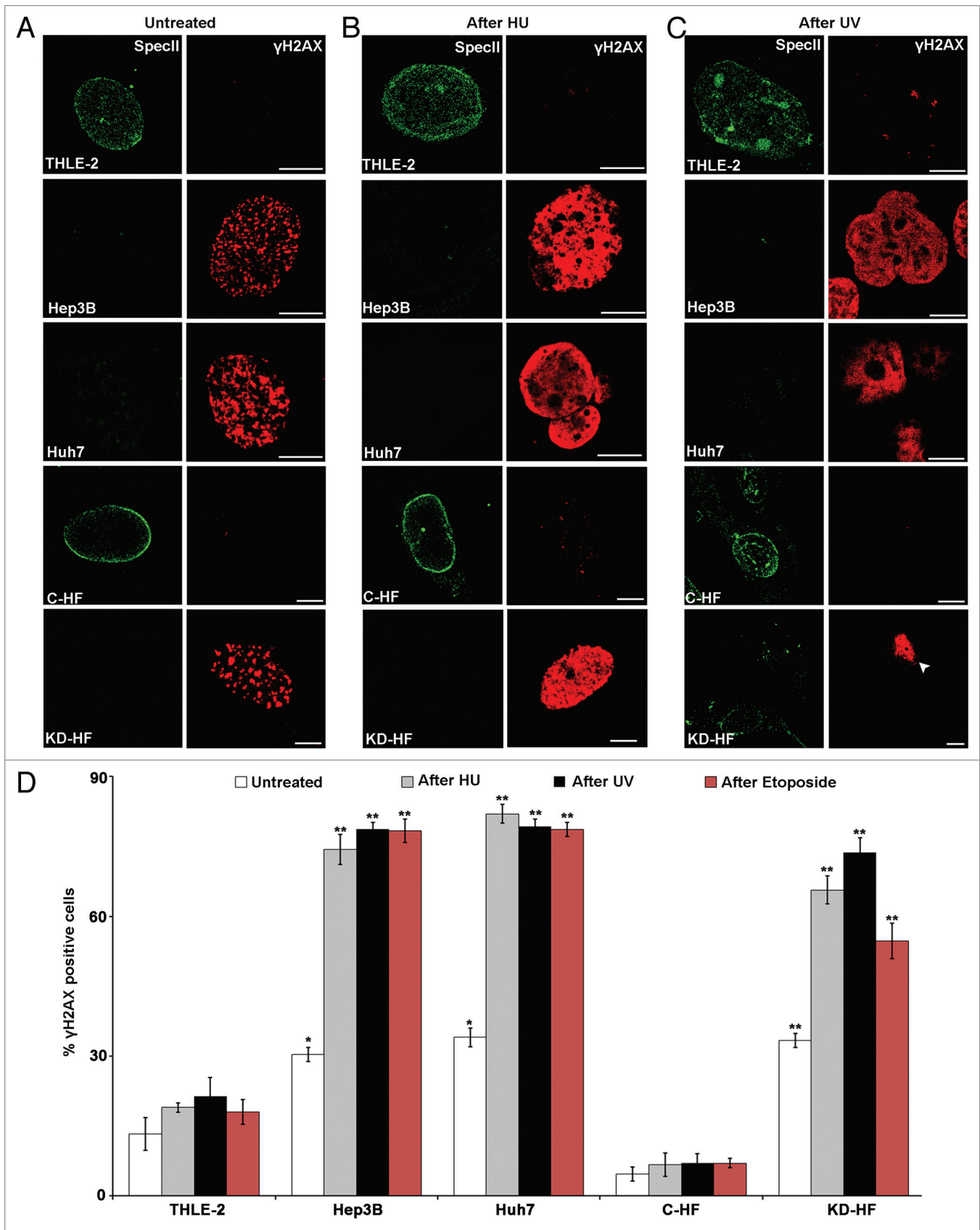


**Figure 6.** For figure legend, see page 187.

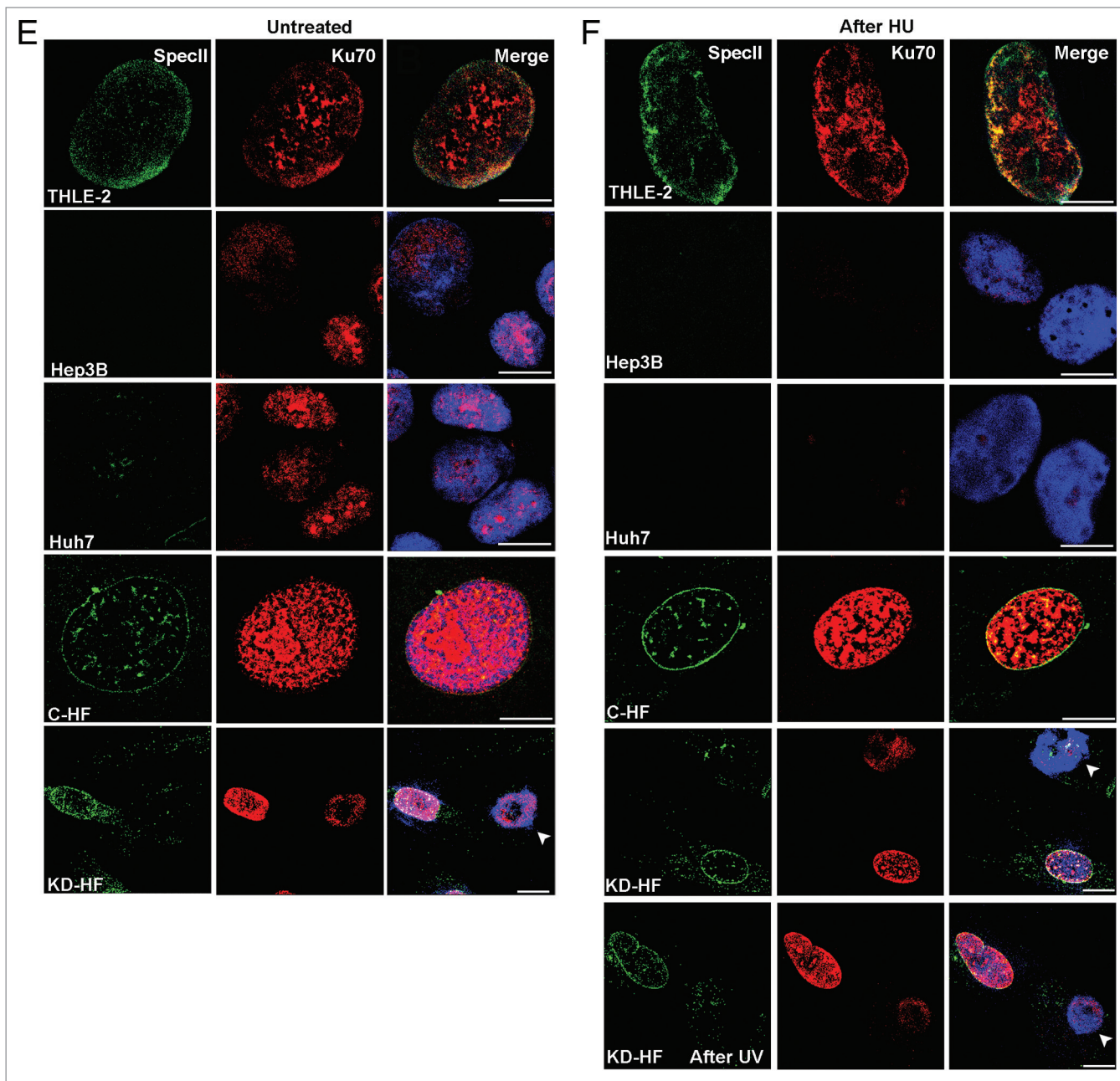


**Figure 6 (See opposite page)** Nesprin-1 is required for an efficient NHEJ. **(A, B, C)** Loss of Nesprin-1 leads to increased  $\gamma$ H2AX staining. Nesprin-1 (pAb Specl1, green) and  $\gamma$ H2AX (red) staining of THLE-2, Hep3B, Huh7, C-HF, and Nesprin-1 KD-HF cells before **(A)**, after HU **(B)**, and after UV treatment **(C)**. Arrow head indicates KD-HF cells after UV treatment. Scale bars, 10  $\mu$ m. **(D)** Quantification of the percentage of cells presenting  $> 5$   $\gamma$ H2AX-labeled foci before (white bar), after (gray bar) HU, after (black bar) UV, after (red bar) Etoposide treatment. Graphs show results from at least three independent experiments. Error bars represent standard deviations ( $*P < 0.001$ ,  $**P < 0.0001$ ). **(E, F)** Immunofluorescence analysis of Ku70 in THLE-2, Hep3B, Huh7, C-HF, and KD-HF cells before **(E)** and after HU and UV **(F)** treatment. pAb Specl1 (green), Ku70 (red), and DAPI (blue). Bottom panels, arrow heads point to Nesprin-1 KD-HF cells. Scale bars, 10  $\mu$ m.

#### Western blotting, pulldown experiments, immunoprecipitation, and blot overlay

Proteins were separated by SDS PAGE and transferred to nitrocellulose membranes for subsequent probing with antibodies. For detection of the Nesprin Giant proteins with molecular masses above 800 000 we separated the proteins by gradient SDS PAGE (2–10% acrylamide) and performed

the transfer in blotting buffer containing (48 mM Tris-HCl, 39 mM glycine, pH 8.3) for 24–72 h as described.<sup>22</sup>

To identify interaction partners of Nesprin-1, GST-Nesprin-1-286 encompassing the ABD of mouse Nesprin-1 was used for pull down experiments.<sup>22</sup> For pull down assays C2F3 cells were lysed in lysis buffer (50 mM Tris-HCl, pH 7.5, 150 mM NaCl, 1% NP-40, 0.5% sodium deoxycholate, 1 mM

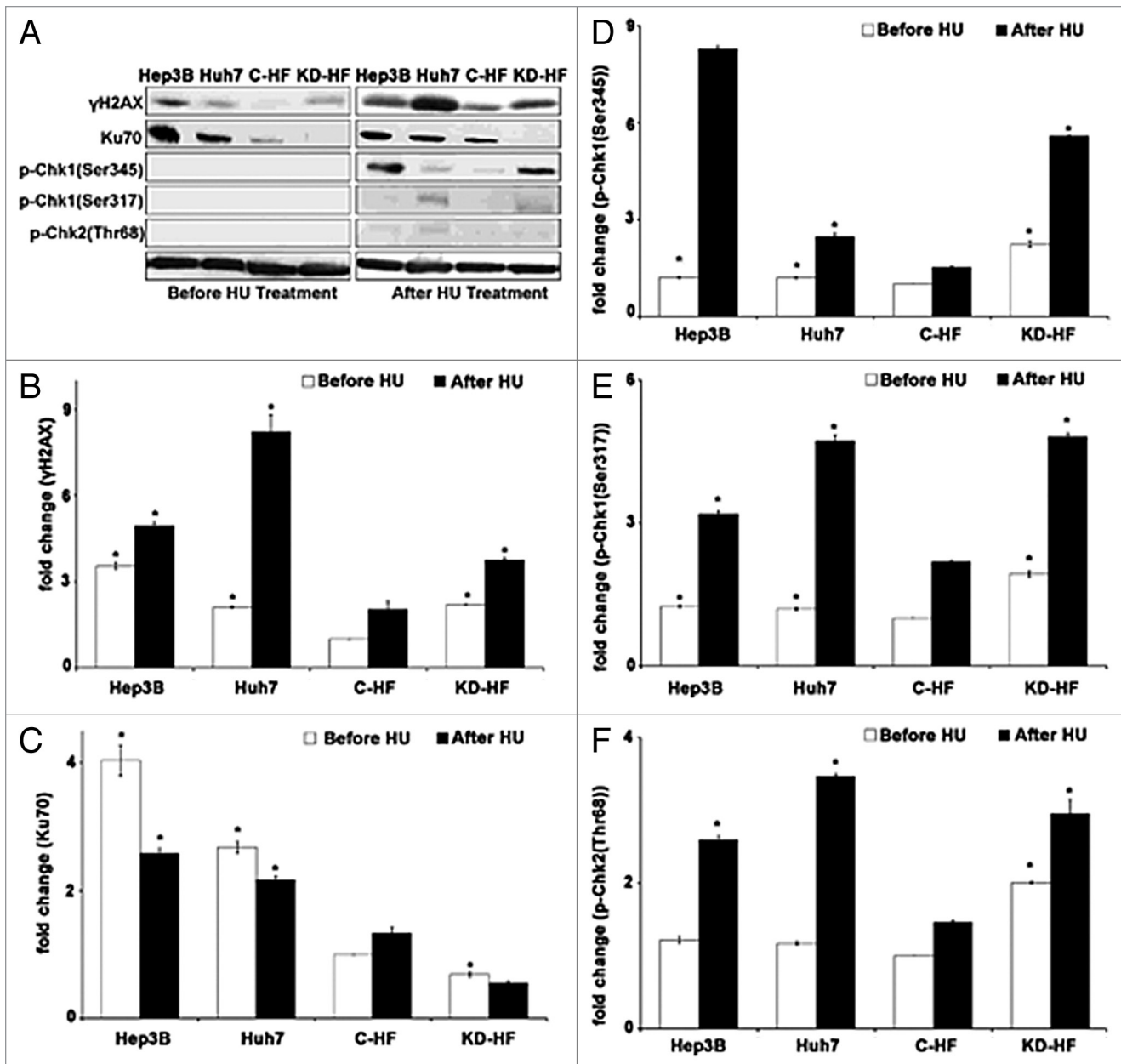


**Figure 7.** Nesprin-1 is involved in the DNA Damage Response network. (A) western blot analysis for determination of levels of  $\gamma$ H2AX (Ser319), CHK1 (Ser345), CHK1 (Ser317), CHK2 (Thr68), and Ku70 before and after HU treatment. Tubulin was used for loading control. (B-F) Histograms representing fold changes of band intensities of H2AX (Ser319), CHK1 (Ser345), and CHK1 (Ser317), CHK2 (Thr68), and Ku70 before (white bar) or after (black bar) HU treatment (compare Fig. 7A). Data are the mean  $\pm$  SD from three samples per group of three independent experiments (\* $P < 0.0001$ ).

DTT, 1 mM benzamidine, and 1 mM PMSF). For preclearing, lysates were incubated with glutathione sepharose beads for one hour at 4 °C followed by incubation with GST-Nesprin-1-286- and GST-bound beads for control. Beads were washed three times with PBS (500 g, 4 °C, 1 min) and boiled in SDS sample buffer (95 °C, 5 min). Samples were separated using 12% SDS polyacrylamide gels and stained with Coomassie brilliant blue R. Protein bands of interest were cut out and subjected to LCMS analysis.

For immunoprecipitation, COS7 cells were transfected with GFP-Nesprin-1-286. The cells were immediately suspended in

1 ml hypotonic buffer (10 mM HEPES, pH 7.9, 1.5 mM MgCl<sub>2</sub>, and 10 mM KCl, PIC (proteinase inhibitor cocktail, Sigma) followed by centrifugation (1000 rpm, 20 s, 4 °C). Pellets were again resuspended in 1 ml hypotonic buffer. Cell suspensions were lysed through a needle (0.4 mm) for 10 times and incubated on ice for 10 min. Nuclear and cytoplasmic fractions were separated by centrifugation (1000 rpm, 10 min, 4 °C). Pellets (nuclear fraction) were washed with 1 ml PBS (1000 rpm, 6  $\times$  10 min, 4 °C). Finally nuclear fractions were pre-cleared with Protein-A-Sepharose CL-4B (Pharmacia Biotech) for 2 h at 4 °C. The samples were incubated for 2 h at 4 °C with GFP-TRAP

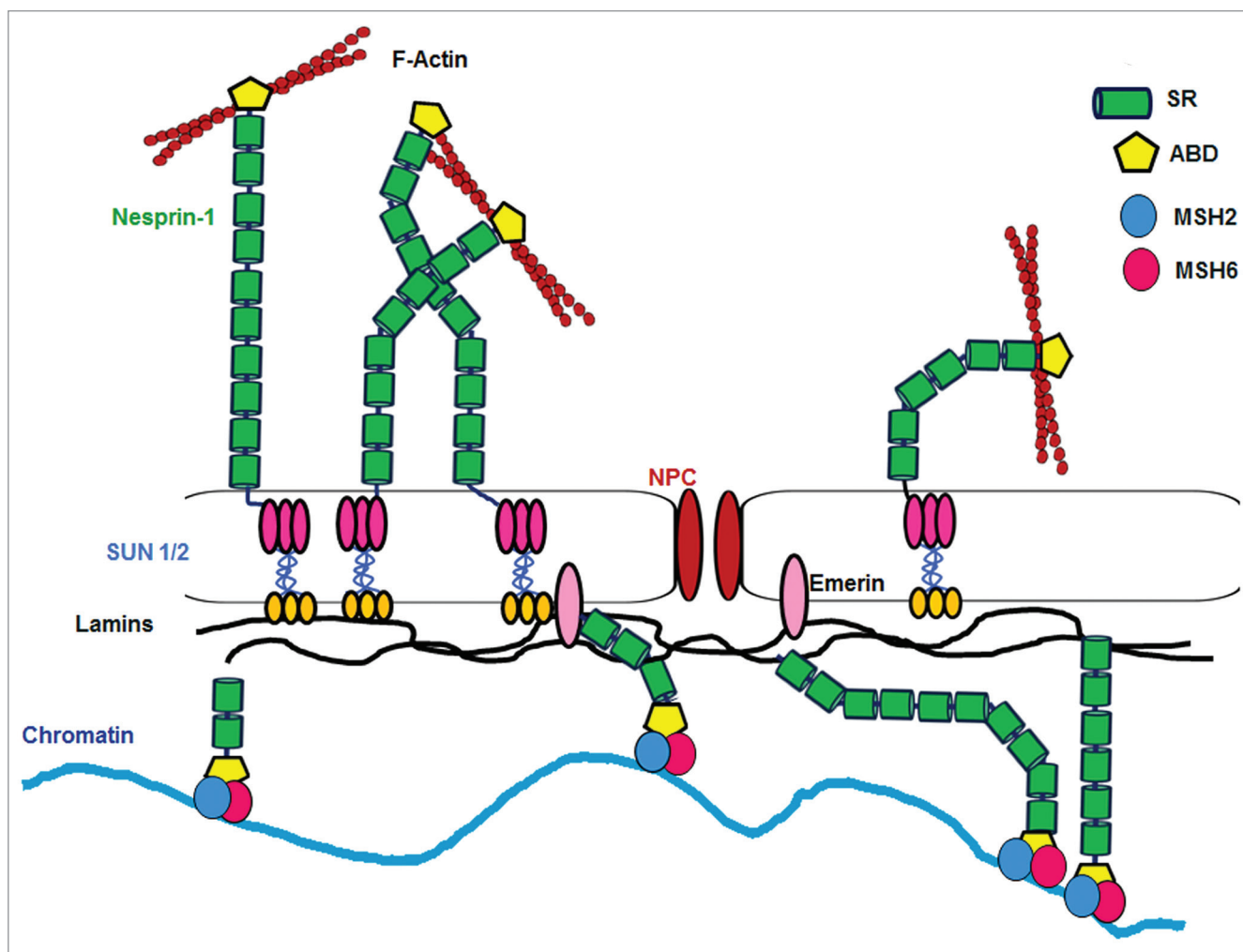


**Figure 8.** Model illustrating Nesprin-1 and MMR interaction. The Nesprin-1 interaction with MSH2 and MSH6 (MutS $\alpha$  complex) is a constitutive cellular event required for proper DNA repair. Therefore, a defect in this interaction chain leads to genome instability.

beads (ChromoTek). Immunocomplexes were washed three times with PBS supplemented with protease inhibitors. The samples from pull down and immunoprecipitations were boiled in SDS sample buffer (95 °C, 5 min) and analyzed by western blot.

The blot overlay was performed according to a published procedure with slight modifications.<sup>62</sup> The samples from immunoprecipitations of GFP-Nesprin-1-286 and GFP were separated by SDS/PAGE and transferred to nitrocellulose membranes. Membranes were blocked with 10 mM Tris-HCl, pH 7.0, 150 mM NaCl, 0.1% (v/v) Tween-20, 0.1% (v/v) NP40, and the blot was rinsed with PBS, 0.1% (v/v) Tween-20 and further incubated with either 5  $\mu$ g/ml GST or GST-MSH2-1-138 protein (diluted in PBS, 0.1% Tween-20) 1 h at 4 °C. Binding of GST-MSH2-1-138 was detected by incubation with anti-GST antibody (Amersham Biosciences) and rabbit anti-goat IgG Ab conjugated to horseradish peroxidase (Sigma), followed by the ECL western blotting detection solution. To obtain recombinant MSH2 polypeptides, we subcloned individual domains for

expression as GST-fusion proteins. The N-terminal sequences reacted with the ABD of Nesprin-1.

#### Miscellaneous methods

RNA isolation, cDNA generation, subcellular fractionation and quantitative RT-PCR analysis were done as described.<sup>23</sup> Primer sequences designed for RT-PCR analysis for Nesprin-1, MSH2, and MSH6 cDNA amplification are listed in Table S2. Cell synchronization was performed according to Li et al.<sup>35</sup> FACS cell sorting was performed at the central facilities of the CMMC.

The cell sensitivity of C-HF, KD-HF, and DLD-1 cells to Etoposide was tested by 3-(4,5-dimethylthiazol-2-yl)-2,5-diphenyltetrazolium bromide (MTT) colorimetric assay as described previously.<sup>36</sup> Briefly, C-HF, KD-HF, and DLD-1 cells were treated with different concentrations of the Etoposide ranging from 10<sup>-8</sup> M to 10<sup>-4</sup> M for 5 d. On day 5, 10  $\mu$ l MTT (5 mg/ml, Sigma) was added to each well and cells were incubated for an additional 4 h at 37 °C. The (IC<sub>50</sub>) value was determined

as the concentration of Etoposide which produced 50% growth inhibition of absorbance at 570 nm.

To assay for DNA damage response, the cells were grown for 24 h in 500  $\mu$ M HU, and 20  $\mu$ M Etoposide or treated with 20 J/m<sup>2</sup> UV.<sup>63</sup> The HU treated cells were processed for immunofluorescence and western blot analysis, Etoposide or UV exposed cells were processed for immunofluorescence.

#### Disclosure of Potential Conflicts of Interests

No potential conflict of interest was disclosed.

#### References

1. Shimi T, Butin-Israeli V, Goldman RD. The functions of the nuclear envelope in mediating the molecular crosstalk between the nucleus and the cytoplasm. *Curr Opin Cell Biol* 2012; 24:71-8; PMID:22192274; <http://dx.doi.org/10.1016/j.ccb.2011.11.007>
2. Maraldi NM, Lattanzi G, Cenni V, Bavelloni A, Marmioli S, Manzoli FA. Laminopathies and A-type lamin-associated signalling pathways. *Adv Enzyme Regul* 2010; 50:248-61; PMID:19917303; <http://dx.doi.org/10.1016/j.advenzreg.2009.10.019>
3. Schirmer EC, Florens L, Guan T, Yates JR 3rd, Gerace L. Nuclear membrane proteins with potential disease links found by subtractive proteomics. *Science* 2003; 301:1380-2; PMID:12958361; <http://dx.doi.org/10.1126/science.1088176>
4. Therizols P, Fairhead C, Cabal GG, Genovesio A, Olivo-Marin JC, Dujon B, Fabre E. Telomere tethering at the nuclear periphery is essential for efficient DNA double strand break repair in subtelomeric region. *J Cell Biol* 2006; 172:189-99; PMID:16418532; <http://dx.doi.org/10.1083/jcb.200505159>
5. Chow KH, Factor RE, Ullman KS. The nuclear envelope environment and its cancer connections. *Nat Rev Cancer* 2012; 12:196-209; PMID:22337151
6. Padmakumar VC, Libotte T, Lu W, Zaim H, Abraham S, Noegel AA, Gotzmann J, Foisner R, Karakesisoglou I. The inner nuclear membrane protein Sun1 mediates the anchorage of Nesprin-2 to the nuclear envelope. *J Cell Sci* 2005; 118:3419-30; PMID:16079285; <http://dx.doi.org/10.1242/jcs.02471>
7. Zhang Q, Bethmann C, Worth NF, Davies JD, Wasner C, Feuer A, Ragnauth CD, Yi Q, Mellad JA, Warren DT, et al. Nesprin-1 and -2 are involved in the pathogenesis of Emery Dreifuss muscular dystrophy and are critical for nuclear envelope integrity. *Hum Mol Genet* 2007; 16:2816-33; PMID:17761684; <http://dx.doi.org/10.1093/hmg/ddm238>
8. Gros-Louis F, Dupré N, Dion P, Fox MA, Laurent S, Verreault S, Sanes JR, Bouchard JP, Rouleau GA. Mutations in SYNE1 lead to a newly discovered form of autosomal recessive cerebellar ataxia. *Nat Genet* 2007; 39:80-5; PMID:17159980; <http://dx.doi.org/10.1038/ng1927>
9. Attali R, Warwar N, Israel A, Gurt I, McNally E, Puckelwartz M, Glick B, Nevo Y, Ben-Neriah Z, Melki J. Mutation of SYNE-1, encoding an essential component of the nuclear lamina, is responsible for autosomal recessive arthrogryposis. *Hum Mol Genet* 2009; 18:3462-9; PMID:19542096; <http://dx.doi.org/10.1093/hmg/ddp290>
10. Grady RM, Starr DA, Ackerman GL, Sanes JR, Han M. Syne proteins anchor muscle nuclei at the neuromuscular junction. *Proc Natl Acad Sci U S A* 2005; 102:4359-64; PMID:15749817; <http://dx.doi.org/10.1073/pnas.0500711102>

11. Banerjee I, Zhang J, Moore-Morris T, Pfeiffer E, Buchholz KS, Liu A, Ouyang K, Stroud MJ, Gerace L, Evans SM, et al. Targeted ablation of nesprin 1 and nesprin 2 from murine myocardium results in cardiomyopathy, altered nuclear morphology and inhibition of the biomechanical gene response. *PLoS Genet* 2014; 10:e1004114; PMID:24586179; <http://dx.doi.org/10.1371/journal.pgen.1004114>
12. Puckelwartz MJ, Kessler E, Zhang Y, Hodzic D, Randles KN, Morris G, Earley JU, Hadhazy M, Holaska JM, Mewborn SK, et al. Disruption of nesprin-1 produces an Emery Dreifuss muscular dystrophy-like phenotype in mice. *Hum Mol Genet* 2009; 18:607-20; PMID:19008300; <http://dx.doi.org/10.1093/hmg/ddn386>
13. Zhang J, Felder A, Liu Y, Guo LT, Lange S, Dalton ND, Gu Y, Peterson KL, Mizisin AP, Shelton GD, et al. Nesprin 1 is critical for nuclear positioning and anchorage. *Hum Mol Genet* 2010; 19:329-41; PMID:19864491; <http://dx.doi.org/10.1093/hmg/ddp499>
14. Chancellor TJ, Lee J, Thodeti CK, Lele T. Actomyosin tension exerted on the nucleus through nesprin-1 connections influences endothelial cell adhesion, migration, and cyclic strain-induced reorientation. *Biophys J* 2010; 99:115-23; PMID:20655839; <http://dx.doi.org/10.1016/j.bpj.2010.04.011>
15. Marmé A, Zimmermann HP, Moldenhauer G, Schorpp-Kistner M, Müller C, Keberlein O, Giersch A, Kretschmer J, Seib B, Spiess E, et al. Loss of Drop1 expression already at early tumor stages in a wide range of human carcinomas. *Int J Cancer* 2008; 123:2048-56; PMID:18709643; <http://dx.doi.org/10.1002/ijc.23763>
16. Doherty JA, Rossing MA, Cushing-Haugen KL, Chen C, Van Den Berg DJ, Wu AH, Pike MC, Ness RB, Moysich K, Chenevix-Trench G, et al.; Australian Ovarian Cancer Study Management Group; Australian Cancer Study (Ovarian Cancer); Ovarian Cancer Association Consortium (OCAC). ESR1/SYNE1 polymorphism and invasive epithelial ovarian cancer risk: an Ovarian Cancer Association Consortium study. *Cancer Epidemiol Biomarkers Prev* 2010; 19:245-50; PMID:20056644; <http://dx.doi.org/10.1158/1055-9965.EPI-09-0729>
17. Sjöblom T, Jones S, Wood LD, Parsons DW, Lin J, Barber TD, Mandelker D, Leary RJ, Ptak J, Silliman N, et al. The consensus coding sequences of human breast and colorectal cancers. *Science* 2006; 314:268-74; PMID:16959974; <http://dx.doi.org/10.1126/science.1133427>
18. Tessema M, Willink R, Do K, Yu YY, Yu W, Machida EO, Brock M, Van Neste L, Stidley CA, Baylin SB, et al. Promoter methylation of genes in and around the candidate lung cancer susceptibility locus 6q23-25. *Cancer Res* 2008; 68:1707-14; PMID:18339850; <http://dx.doi.org/10.1158/0008-5472.CAN-07-6325>
19. Schuebel KE, Chen W, Cope L, Glöckner SC, Suzuki H, Yi JM, Chan TA, Van Neste L, Van Criekinge W, van den Bosch S, et al. Comparing the DNA hypermethylome with gene mutations in human colorectal cancer. *PLoS Genet* 2007; 3:1709-23; PMID:17892325; <http://dx.doi.org/10.1371/journal.pgen.0030157>

#### Acknowledgments

We thank to Dr Reena Buurman for providing the THLE-2 cells. We thank Drs R Rastetter and MS Hussain for help at various stages of this work, Dr VS Peche and P Li for providing material, and Berthold Gaßen for providing antibodies. The work was supported by CECAD.

#### Supplemental Materials

Supplemental materials may be found here:

[www.landesbioscience.com/journals/nucleus/article/29023](http://www.landesbioscience.com/journals/nucleus/article/29023)

20. Masica DL, Karchin R. Correlation of somatic mutation and expression identifies genes important in human glioblastoma progression and survival. *Cancer Res* 2011; 71:4550-61; PMID:21555372; <http://dx.doi.org/10.1158/0008-5472.CAN-11-0180>
21. Rajgor D, Mellad JA, Autore F, Zhang Q, Shanahan CM. Multiple novel nesprin-1 and nesprin-2 variants act as versatile tissue-specific intracellular scaffolds. *PLoS One* 2012; 7:e40098; PMID:22768332; <http://dx.doi.org/10.1371/journal.pone.0040098>
22. Taranum S, Sur I, Müller R, Lu W, Rashmi RN, Munck M, Neumann S, Karakesisoglou I, Noegel AA. Cytoskeletal interactions at the nuclear envelope mediated by nesprins. *Int J Cell Biol* 2012; 2012:736524; PMID:22518138; <http://dx.doi.org/10.1155/2012/736524>
23. Taranum S, Vaylann E, Meinke P, Abraham S, Yang L, Neumann S, Karakesisoglou I, Wehnert M, Noegel AA. LINC complex alterations in DMD and EDMD/CMT fibroblasts. *Eur J Cell Biol* 2012; 91:614-28; PMID:22555292; <http://dx.doi.org/10.1016/j.ejcb.2012.03.003>
24. Dechat T, Gajewski A, Korbei B, Gerlich D, Daigle N, Haraguchi T, Furukawa K, Ellenberg J, Foisner R. LAP2alpha and BAF transiently localize to telomeres and specific regions on chromatin during nuclear assembly. *J Cell Sci* 2004; 117:6117-28; PMID:15546916; <http://dx.doi.org/10.1242/jcs.01529>
25. Dorner D, Vleck S, Foeger N, Gajewski A, Makolm C, Gotzmann J, Hutchinson CJ, Foisner R. Lamina-associated polypeptide 2alpha regulates cell cycle progression and differentiation via the retinoblastoma-E2F pathway. *J Cell Biol* 2006; 173:83-93; PMID:16606692; <http://dx.doi.org/10.1083/jcb.200511149>
26. Strambio-De-Castillia C, Niepel M, Rout MP. The nuclear pore complex: bridging nuclear transport and gene regulation. *Nat Rev Mol Cell Biol* 2010; 11:490-501; PMID:20571586; <http://dx.doi.org/10.1038/nrm2928>
27. Chatel G, Fahrenkrog B. Dynamics and diverse functions of nuclear pore complex proteins. *Nucleus* 2012; 3:162-71; PMID:22555605; <http://dx.doi.org/10.4161/nucl.19674>
28. Martínez N, Alonso A, Moragues MD, Pontón J, Schneider J. The nuclear pore complex protein Nup88 is overexpressed in tumor cells. *Cancer Res* 1999; 59:5408-11; PMID:10554006
29. Agudo D, Gómez-Esquer F, Martínez-Arribas F, Núñez-Villar MJ, Pollán M, Schneider J. Nup88 mRNA overexpression is associated with high aggressiveness of breast cancer. *Int J Cancer* 2004; 109:717-20; PMID:14999780; <http://dx.doi.org/10.1002/ijc.20034>
30. Zhang ZY, Zhao ZR, Jiang L, Li JC, Gao YM, Cui DS, Wang CJ, Schneider J, Wang MW, Sun XF. Nup88 expression in normal mucosa, adenoma, primary adenocarcinoma and lymph node metastasis in the colorectum. *Tumour Biol* 2007; 28:93-9; PMID:17264541; <http://dx.doi.org/10.1159/000099154>

31. Brustmann H, Hager M. Nucleoporin 88 expression in normal and neoplastic squamous epithelia of the uterine cervix. *Ann Diagn Pathol* 2009; 13:303-7; PMID:19751906; <http://dx.doi.org/10.1016/j.anndiagpath.2009.05.005>
32. Schneider J, Martínez-Arribas F, Torrejón R. Nup88 expression is associated with myometrial invasion in endometrial carcinoma. *Int J Gynecol Cancer* 2010; 20:804-8; PMID:20973273; <http://dx.doi.org/10.1111/IGC.0b013e3181dfaa6b>
33. Emterling A, Skoglund J, Arbman G, Schneider J, Evertsson S, Carstensen J, Zhang H, Sun XF. Clinicopathological significance of Nup88 expression in patients with colorectal cancer. *Oncology* 2003; 64:361-9; PMID:12759533; <http://dx.doi.org/10.1159/000070294>
34. Warren JJ, Pohlhaus TJ, Changela A, Iyer RR, Modrich PL, Beese LS. Structure of the human MutSalpha DNA lesion recognition complex. *Mol Cell* 2007; 26:579-92; PMID:17531815; <http://dx.doi.org/10.1016/j.molcel.2007.04.018>
35. Li F, Mao G, Tong D, Huang J, Gu L, Yang W, Li GM. The histone mark H3K36me3 regulates human DNA mismatch repair through its interaction with MutS $\alpha$ . *Cell* 2013; 153:590-600; PMID:23622243; <http://dx.doi.org/10.1016/j.cell.2013.03.025>
36. Jacob S, Aguado M, Fallik D, Praz F. The role of the DNA mismatch repair system in the cytotoxicity of the topoisomerase inhibitors camptothecin and etoposide to human colorectal cancer cells. *Cancer Res* 2001; 61:6555-62; PMID:11522654
37. Aebi S, Fink D, Gordon R, Kim HK, Zheng H, Fink JL, Howell SB. Resistance to cytotoxic drugs in DNA mismatch repair-deficient cells. *Clin Cancer Res* 1997; 3:1763-7; PMID:9815561
38. de las Alas MM, Aebi S, Fink D, Howell SB, Los G. Loss of DNA mismatch repair: effects on the rate of mutation to drug resistance. *J Natl Cancer Inst* 1997; 89:1537-41; PMID:9337351; <http://dx.doi.org/10.1093/jnci/89.20.1537>
39. Shahi A, Lee JH, Kang Y, Lee SH, Hyun JW, Chang IY, Jun JY, You HJ. Mismatch-repair protein MSH6 is associated with Ku70 and regulates DNA double-strand break repair. *Nucleic Acids Res* 2011; 39:2130-43; PMID:21075794; <http://dx.doi.org/10.1093/nar/gkq1095>
40. Villemure JF, Abaji C, Cousineau I, Belmaaza A. MSH2-deficient human cells exhibit a defect in the accurate termination of homology-directed repair of DNA double-strand breaks. *Cancer Res* 2003; 63:3334-9; PMID:12810667
41. Marti TM, Hefner E, Feeny L, Natale V, Cleaver JE. H2AX phosphorylation within the G1 phase after UV irradiation depends on nucleotide excision repair and not DNA double-strand breaks. *Proc Natl Acad Sci U S A* 2006; 103:9891-6; PMID:16788066; <http://dx.doi.org/10.1073/pnas.0603779103>
42. Liu Q, Guntuku S, Cui XS, Matsuoka S, Cortez D, Tamaï K, Luo G, Carattini-Rivera S, DeMayo F, Bradley A, et al. Chk1 is an essential kinase that is regulated by Atr and required for the G(2)/M DNA damage checkpoint. *Genes Dev* 2000; 14:1448-59; PMID:10859164
43. Kastan MB, Lim DS. The many substrates and functions of ATM. *Nat Rev Mol Cell Biol* 2000; 1:179-86; PMID:11252893; <http://dx.doi.org/10.1038/35043058>
44. Sun J, Lee KJ, Davis AJ, Chen DJ. Human Ku70/80 protein blocks exonuclease 1-mediated DNA resection in the presence of human Mre11 or Mre11/Rad50 protein complex. *J Biol Chem* 2012; 287:4936-45; PMID:22179609; <http://dx.doi.org/10.1074/jbc.M111.306167>
45. Liang F, Jasin M. Ku80-deficient cells exhibit excess degradation of extrachromosomal DNA. *J Biol Chem* 1996; 271:14405-11; PMID:8662903; <http://dx.doi.org/10.1074/jbc.271.24.14405>
46. Downs JA, Jackson SP. A means to a DNA end: the many roles of Ku. *Nat Rev Mol Cell Biol* 2004; 5:367-78; PMID:15122350; <http://dx.doi.org/10.1038/nrm1367>
47. Capo-chichi CD, Cai KQ, Testa JR, Godwin AK, Xu XX. Loss of GATA6 leads to nuclear deformation and aneuploidy in ovarian cancer. *Mol Cell Biol* 2009; 29:4766-77; PMID:19581290; <http://dx.doi.org/10.1128/MCB.00087-09>
48. Goldman RD, Shumaker DK, Erdos MR, Eriksson M, Goldman AE, Gordon LB, Gruenbaum Y, Khuon S, Mendez M, Varga R, et al. Accumulation of mutant lamin A causes progressive changes in nuclear architecture in Hutchinsonin-Gilford progeria syndrome. *Proc Natl Acad Sci U S A* 2004; 101:8963-8; PMID:15184648; <http://dx.doi.org/10.1073/pnas.0402943101>
49. Cao K, Capell BC, Erdos MR, Djabali K, Collins FS. A lamin A protein isoform overexpressed in Hutchinsonin-Gilford progeria syndrome interferes with mitosis in progeria and normal cells. *Proc Natl Acad Sci U S A* 2007; 104:4949-54; PMID:17360355; <http://dx.doi.org/10.1073/pnas.0611640104>
50. Chen CY, Chi YH, Mutalif RA, Starost MF, Myers TG, Anderson SA, Stewart CL, Jeang KT. Accumulation of the inner nuclear envelope protein Sun1 is pathogenic in progeric and dystrophic laminopathies. *Cell* 2012; 149:565-77; PMID:22541428; <http://dx.doi.org/10.1016/j.cell.2012.01.059>
51. Sherr CJ. Principles of tumor suppression. *Cell* 2004; 116:235-46; PMID:14744434; [http://dx.doi.org/10.1016/S0092-8674\(03\)01075-4](http://dx.doi.org/10.1016/S0092-8674(03)01075-4)
52. Clifford B, Beljin M, Stark GR, Taylor WR. G2 arrest in response to topoisomerase II inhibitors: the role of p53. *Cancer Res* 2003; 63:4074-81; PMID:12874009
53. Lei K, Zhu X, Xu R, Shao C, Xu T, Zhuang Y, Han M. Inner nuclear envelope proteins SUN1 and SUN2 play a prominent role in the DNA damage response. *Curr Biol* 2012; 22:1609-15; PMID:22863315; <http://dx.doi.org/10.1016/j.cub.2012.06.043>
54. Pena-Diaz J, Bregenhorn S, Ghodgaonkar M, Follonier C, Artola-Boran M, Castor D, et al. Noncanonical Mismatch Repair as a Source of Genomic Instability in Human Cells. *Mol Cell* 2012; 47:669-80
55. Young LC, Hays JB, Tron VA, Andrew SE. DNA mismatch repair proteins: potential guardians against genomic instability and tumorigenesis induced by ultraviolet photoproducts. *J Invest Dermatol* 2003; 121:435-40; PMID:12925197; <http://dx.doi.org/10.1046/j.1523-1747.2003.12450.x>
56. Schofield MJ, Hsieh P. DNA mismatch repair: molecular mechanisms and biological function. *Annu Rev Microbiol* 2003; 57:579-608; PMID:14527292; <http://dx.doi.org/10.1146/annurev.micro.57.030502.090847>
57. di Pietro M, Sabates Bellver J, Menigatti M, Bannwart F, Schneider A, Russell A, Truninger K, Jiricny J, Marra G. Defective DNA mismatch repair determines a characteristic transcriptional profile in proximal colon cancers. *Gastroenterology* 2005; 129:1047-59; PMID:16143142; <http://dx.doi.org/10.1053/j.gastro.2005.06.028>
58. Peters AC, Young LC, Maeda T, Tron VA, Andrew SE. Mammalian DNA mismatch repair protects cells from UVB-induced DNA damage by facilitating apoptosis and p53 activation. *DNA Repair (Amst)* 2003; 2:427-35; PMID:12606123; [http://dx.doi.org/10.1016/S1568-7864\(03\)00003-X](http://dx.doi.org/10.1016/S1568-7864(03)00003-X)
59. Oza P, Jaspersen SL, Miele A, Dekker J, Peterson CL. Mechanisms that regulate localization of a DNA double-strand break to the nuclear periphery. *Genes Dev* 2009; 23:912-27; PMID:19390086; <http://dx.doi.org/10.1101/gad.1782209>
60. Buurman R, Grlevik E, Schffler V, Eilers M, Sandbothe M, Kreipe H, Wilkens L, Schlegelberger B, Khnel F, Skawran B. Histone deacetylases activate hepatocyte growth factor signaling by repressing microRNA-449 in hepatocellular carcinoma cells. *Gastroenterology* 2012; 143:811, e1-15; PMID:22641068; <http://dx.doi.org/10.1053/j.gastro.2012.05.033>
61. Paddison PJ, Caudy AA, Bernstein E, Hannon GJ, Conklin DS. Short hairpin RNAs (shRNAs) induce sequence-specific silencing in mammalian cells. *Genes Dev* 2002; 16:948-58; PMID:11959843; <http://dx.doi.org/10.1101/gad.981002>
62. Wheeler MA, Davies JD, Zhang Q, Emerson LJ, Hunt J, Shanahan CM, Ellis JA. Distinct functional domains in nesprin-1alpha and nesprin-2beta bind directly to emerin and both interactions are disrupted in X-linked Emery-Dreifuss muscular dystrophy. *Exp Cell Res* 2007; 313:2845-57; PMID:17462627; <http://dx.doi.org/10.1016/j.yexcr.2007.03.025>
63. Zinkel SS, Hurov KE, Ong C, Abtahi FM, Gross A, Korsmeyer SJ. A role for proapoptotic BID in the DNA-damage response. *Cell* 2005; 122:579-91; PMID:16122425; <http://dx.doi.org/10.1016/j.cell.2005.06.022>